# Contrasted impact of two macrofaunal species (Hediste diversicolor and Scrobicularia plana) on microphytobenthos spatial distribution and photosynthetic activity at microscale

Jerome Morelle, Olivier Maire, Anais Richard, Alex Slimani, Francis Orvain

# Article Title: Contrasted impact of two macrofaunal species (*Hediste diversicolor* and *Scrobicularia plana*) on microphytobenthos spatial distribution and photosynthetic activity at microscale

**Authors:** Jérôme Morelle[1, 3*], Olivier Maire[2], Anaïs Richard[2], Alex Slimani[1] & Francis Orvain[1]

**Authors affiliations :**
[1] Univ. Normandie, Univ. Caen Normandie, FRE 2030 BOREA, CNRS-7208, IRD-207, MNHN, UPMC, UCBN, UA. Caen, France.
[2] Univ. Bordeaux, UMR 5805 EPOC UMR - OASU. Arcachon, France.
[3] present address: UMR CNRS 6553 ECOBIO. Rennes, France.

*Corresponding author: jerome.morelle@univ-rennes1.fr

## Abstract
Microphytobenthos is most often the primary source of carbon for coastal soft-sediment communities, especially in intertidal and shallow subtidal environments. The influence of benthic macrofaunal organisms on microphytobenthic biomass, spatial distribution and photosynthetic capacities is not only resulting from their feeding intensity but also indirectly from their bioturbation activity, which regulates nutrient fluxes and sediment mixing. This study compares the impact of two species (*Hediste diversicolor* and *Scrobicularia plana*) that dominate macrofaunal communities in estuarine intertidal mudflats on microphytobenthic biomass and photosynthetic activity. Imaging-PAM fluorescence was used to non-invasively map the development of microphytobenthic biomass and to assess its spatial extent. Our results showed that, due to intense deposit feeding, *Scrobicularia plana* quickly limited microphytobenthos growth and photosynthetic activity, even at low density (< 250 ind $m^{-2}$). In contrast, the negative impact of *Hediste diversicolor* on microphytobenthos development due to direct consumption was very low. Thereby, the stimulation of nutrient fluxes at the sediment-water interface resulting from bioirrigation seems to enhance microphytobenthos growth and photosynthesis.

## Keywords:
Imaging-PAM; macrofauna; microphytobenthos; spatial distribution; photosynthesis;

## 1. Introduction

Microphytobenthic assemblages are composed of photosynthetic microalgae (mostly diatoms), cyanobacteria, and flagellates that form a biofilm at the surface of soft-bottom substrates. With a high net production rate, microphytobenthos (MPB) represents the main source of carbon for benthic communities inhabiting coastal shallow environments (Underwood and Kromkamp 1999). Intertidal mudflats fueled by a high MPB primary production can support very high densities of benthic invertebrates and thus often constitute privileged feeding areas for a wide range of predators such as shrimp, fish and shorebirds (Dauvin and Desroy 2005; Kuwae et al. 2008; Saint-Béat et al. 2013). Mudflats also play a transient role as a nursery or refuge for numerous benthic invertebrates, pelagic juvenile fish and migratory species (Hughes *et al.* 2014). The influence of benthic macrofauna or meiofauna on the biomass, spatial distribution and production rate of MPB not only results from their feeding activity (i.e., grazing pressure) but also depends on their effects on organic matter mineralization rates and nutrient cycling, mainly through sediment bioturbation (Swanberg 1991; D'Hondt *et al.* 2018). Altogether, bioturbation processes (i.e. both sediment reworking and bioirrigation) increase the incorporation and regeneration rates of organic carbon within the benthic compartment, thereby stimulating nutrient fluxes across the sediment-water interface where microbenthic primary producers can assimilate them for photosynthesis under optimal conditions (Eriksson et al. 2017; Hope et al. 2020).

Until recently, microphytobenthic primary production was considered to be mainly regulated by temperature and light penetration into the sediment, with a low impact of inorganic nutrient concentrations compared to phytoplankton (Guarini et al. 2000; Savelli et al. 2018). Thereby, a progressive increase in primary production of intertidal MPB was demonstrated up to an optimum temperature beyond which production declined rapidly (Blanchard et al. 1996). In addition, many studies have shown that variations in light penetration at the sediment surface of intertidal mudflats, linked to the tidal cycle, sediment characteristics, and the vertical distribution of biofilm, strongly influence microphytobenthic production (Serôdio 2003; Forster and Kromkamp 2004; Jesus et al. 2009; Serôdio et al. 2012; Cartaxana et al. 2013; Morelle et al. 2018a). However, it is now clearly established that nutrient availability at the sediment-water interface can also profoundly impact primary production rates (An and Joye 2001; Paterson and Hagerthey 2001; Ní Longphuirt et al. 2009; Hochard et al. 2010; Rakotomalala et al. 2019). Indeed, when concentration of nutrients at the sediment-water interface is low, epipelic diatoms, the main components of MPB, are able to migrate vertically to reach the subsurface layers where nutrients resulting from the bacterial mineralization of organic matter accumulate (Froelich et al. 1979; Henrichs 1992; Paterson and Hagerthey 2001; Rakotomalala et al. 2019). During their migration, diatoms gradually move away from the photic layer (Saburova and Polikarpov 2003; Cartaxana et al. 2016), which thus limits photosynthesis and hence microphytobenthic primary production.

In many temperate brackish intertidal areas, *Hediste diversicolor* and *Scrobicularia plana* are dominant species of benthic macrofauna communities, which are also likely to strongly influence microphytobenthic assemblages through both deposit-feeding and bioturbation activities (Ysebaert and Herman 2002; Bergayou et al. 2019). On one hand, as the diet of these two organisms is mainly composed of MPB (Rossi et al. 2015), their grazing

activity would strongly affect its spatial distribution and thus its photosynthetic capacities. On the other hand, through their bioirrigation activity, the two species may have a positive effect on MPB photosynthesis and growth by enhancing remineralization processes and nutrient fluxes across the benthic interface (Thrush et al. 2006; Sandwell et al. 2009; Lohrer et al. 2010; Donadi et al. 2013; Volkenborn et al. 2016; Eriksson et al. 2017). In addition, reworking of the sediment surface may have a negative effect on microphytobenthic development by destabilizing the biofilm, thus increasing the resuspension of unicellular algae and bacteria (Orvain 2005; Kristensen et al. 2013; Savelli et al. 2019).

Both these negative and positive effects of the presence of bioturbators on MPB may considerably vary with the macrofaunal density. The density of these two species should be especially taken into consideration since it can fluctuate markedly both seasonally and spatially (Scaps 2002; Santos et al. 2011), even at mesoscale (i.e. at the scale of a mudflat), and may consequently profoundly modulate their impact on microphytobenthic biofilm development and distribution. In the case of *Hediste diversicolor*, high density lead to greater modification of sediment properties, promoting both biogeochemical fluxes *via* bioirrigation and sediment stability *via* mucus secretion, leading to synergistic effects on MPB (Passarelli *et al.* 2012). Indeed, macrofaunal bioturbation rates and their effects on microbial communities such as bacteria and MPB, and hence on associated processes such as remineralization rates and photosynthesis, tend to increase proportionally with the density of benthic macrofauna as long as no competition occurs (Kristensen 2001). However, the density-dependent relationships in bioturbation remain difficult to predict, particularly in deposit-feeders, as trophic interactions and/or territory competition, occurring when densities exceed a species-dependent threshold (Reible and Mohanty 2002), may profoundly alter feeding and locomotion behaviors. For example, Miron et al. (1991) reported an individual extension of the prospecting area when the density of *Nereis virens* increased while, on the contrary, Duport et al. (2006) showed that *H. diversicolor* reduced its feeding intensity and prospecting area at high density. Moreover, impacts of macrofaunal bioturbation on microbial processes seem also dependent from macrofaunal densities as a function of the process and/or on the macrofaunal species considered (Braeckman et al. 2010). This can induce typical hyperbolic function when regarding at the resuspension rate of MPB in relation with macrofaunal densities (Orvain et al. 2004, 2007). Even though field observations were used to study the effect of benthic organisms on the other components of the trophic network (Weerman et al. 2011), autocorrelation and covariance between the different explanatory variables in natural environment hinder the mechanistic understanding of interrelated processes.

The aim of the present study was to experimentally quantify the impact of *Hediste diversicolor* and *Scrobicularia plana* on microphytobenthic biomass and photosynthetic capacities. Given the high but contrasted bioturbation activity of the two studied species, we expected that they would impact biofilm development in different ways (i.e. destabilization vs. stimulation). Furthermore, we hypothesized that the relative importance of positive and negative effects would be density-dependent and thus tested different densities in a range frequently observed in intertidal estuarine mudflats. Our experimental study was performed in an experimental mesocosm allowing to mimic environmental conditions (e.g. tide, light and temperature conditions) of the sampling area. Anticipating that the impact of sediment

bioturbation by benthic infauna on microphytobenthic assemblages would vary at a spatial micro-scale, we used imaging-PAM fluorescence to assess photosynthetic parameters with a very fine resolution, less than 0.5 mm (Ralph *et al.* 2005).

## 2. Material and methods

### 2.1. Experimental design

Approximately 0.5 $m^3$ of the top 15 cm of sediment was collected in winter (February 2018) in the northern mudflat of the Seine estuary (49°27'01.6''N; 0°12'20.0''E; WGS84). Upon arrival in the laboratory, the fresh sediment was sieved through a 2 mm mesh to remove macrofauna and larger particles (shells). It was then kept for two weeks in tanks with seawater from the sampling site, at constant temperature (12°C) and in total darkness to avoid development of photosynthetic species. The sediment was then divided into 21 experimental units (PVC tube, height 30 cm, internal diameter 9.3 cm) placed in a large tank containing natural seawater (500 L, 12 °C, 17 PSU) with an artificial tidal cycle (6 h low tide; 6 h high tide). The tidal cycle was generated by pumping about 130 L of water in a second tank, corresponding to a variation in the water level of 12 cm (i.e. the sediment surface of experimental units was 10 cm below and 2 cm above the water surface during high and low tide, respectively). Three replicates of sieved sediment (5 ml) were kept for particle grain size analyses.

Specimens of *H. diversicolor* and *S. plana* were collected by hand at the same time. Adult specimens (shell length comprised between 40 and 43 mm for bivalves and approximatively 9 cm body length for worms) were selected and stored in two separate tanks with natural sediment and aerated seawater from the sampling site placed in a temperature-controlled room (darkness, 12 °C). After two weeks, specimens were deposited at the sediment surface of experimental units. All of them buried in less than two hours. Experiments finally began after a one-week acclimation period. The experimental design comprised seven treatments with three replicates each: one treatment with no macrofauna as a control, six treatments corresponding to three densities of *S. plana* or *H. diversicolor*. The lowest densities (249 ind $m^{-2}$ for both species) corresponded to the ones observed during field sampling at the study site. The intermediate and highest densities (332 - 498 and 498 - 747 ind $m^{-2}$ for *S. plana* and *H. diversicolor*, respectively) were in the range commonly reported for the two species in the literature (Scaps 2002; Santos et al. 2011).

Four days before the beginning of the experiment, microphytobenthic biofilm (i.e. the top 0.5 cm of colonized sediment) was collected on the same site in the northern mudflat of the Seine estuary. Back in the laboratory, the sediment was evenly spread on trays and a 63 µm nylon net was delicately placed onto the surface (Orvain et al. 2003). Trays were then placed under an average light intensity of 114 µmol photons $m^{-2}$ $s^{-1}$ for 3 days, which represents a typical lag phase providing the time for benthic diatom to settle, start migratory cycles, and initiate a new colonization of the sediment surface (Orvain et al. 2003). One day before the beginning of the experiment, the microphytobenthic biofilm was collected by delicately brushing the net and a 0.5 cm layer of sieved sediment inoculated with the biofilm was deposited on the surface of experimental units at intervals of one day between replicates (i.e. one replicate of each treatment per day over a period of three days).

During the diurnal low tide, a neon ramp placed on the top of the tank emitted a spatially homogeneous photons flux. During high tide phases and nocturnal low tide, no artificial light was applied to the surface of experimental units in order to mimic field conditions where turbidity prevents light penetration (Morelle *et al.* 2018b). Light intensities were recorded at one-minute intervals using Onset Hobo UA-002 Pendant light data loggers placed on the surface of two additional units in the tank. Salinity and temperature were measured daily using a multiparameter probe. Photosynthetic parameters were then measured every day at the beginning of the diurnal low tide by chaining the replicated series (one replicate of each treatment per series) using an imaging-PAM fluorometer (Walz, Germany). On the 6$^{th}$ day of each replicated series, the first centimeter of the sediment was sampled and immediately homogenized to measure sediment parameters (water content, volumetric mass and dry bulk density), and biological parameters (Exopolysaccharides, chlorophyll *a* and phaeopigment contents). The sediment column of all experimental units was then sliced to assess the number of live individuals.

### 2.2. Sedimentary parameters and nutrients analyses

To determine particle grain size, sieved sediment samples were digested in 6% hydrogen peroxide for 48 h to remove organic matter. The grain size distribution was then measured on subsamples using a LS Coulter particle size analyzer. The mud sediment fraction was estimated as the percentage of silt particles < 63 µm and the median grain size diameter was estimated using a cumulative percentage histogram.

After sampling, the fresh sediment collected on day 6 was weighted to calculate the volumetric mass (in Kg L$^{-1}$) and conserved at -20°C before further analysis. After freeze-drying (24h), water content (ω; %) was determined as a percentage of water weight relative to otal dry weight. The dry bulk density ($C_{sed}$, kg m$^{-3}$) was estimated from ω according to the following equation:

$$C_{sed} = \frac{(\gamma_s \times 1000)}{\frac{\omega}{100} \times \gamma_s + 1000} \quad (1)$$

where $\gamma_s$ is the grain density of 2,650 kg m$^{-3}$.

### 2.3. Biological parameters

#### 2.3.1. Imaging-PAM fluorescence

*Measurement.* Fluorescence measurements were carried out using the Maxi Version of Imaging-PAM Chlorophyll Fluorometer (Walz, Effeltrich, Germany) associated with a LED-Array Illumination Unit IMAG-MAX/L (44 high-power royal-blue (450 nm) LED-lamps) and a CCD Camera IMAG-K7 equipped with a Zoom objective lens (640 x 480-pixel resolution). Measurements were performed at a fixed working distance of 18.5 cm. After 5 minutes of dark adaptation, which is a compromise between oxidation of the Quinone pool and vertical migration of microphytobenthic cells at depth (Serôdio 2003; Perkins et al. 2010), in each experimental unit, an area of interest (AOI) was selected in which minimal level of fluorescence was maximum. The sample was excited by a low frequency measuring light (1 µmol photons m$^{-2}$ s$^{-1}$, 450 nm) to determine the minimal level of fluorescence (Fo) which represent a proxy for microphytobenthic biomass (Kromkamp and Peene 1999; Jesus et al. 2005). Maximum fluorescence (Fm) was then obtained using a saturating light pulse (0.8s,

6,000 µmol photons $m^{-2}$ $s^{-1}$, 450nm), allowing the Quinone A, Quinone B and part of plastoquinone pools to be reduced. The maximum effective quantum yield of the PSII (Van Kooten and Snel 1990) could then be estimated as Fv/Fm = (Fm-Fo)/Fm. Subsequently, each replicate was exposed to 13 incremental intensities of actinic light (E): 0, 8, 21, 56, 111, 186, 281, 336, 396, 461, 531, 611, and 701 µmol photons $m^{-2}$ $s^{-1}$ with a 30-second irradiance step. At each actinic light step, a steady state fluorescence (Fs) and a new maximum fluorescence (Fm') were measured to enable calculation of the effective quantum yield of PSII (ΔF/Fm'= (Fm'-Fs)/Fm'). Numerical values and fluorescence images were extracted using analytical software (Imaging Win; Walz).

*Image analysis.* To obtain numerical values of fluorescence spatial heterogeneity from the images, a Matlab© routine was developed to determine the values of each level of fluorescence (Fo, Fm, Fs and Fm') for each pixel. Briefly, the images corresponding to all successive actinic light per RLC were nested in a 3D matrix. A value was assigned for each color level and each pixel was converted into a numerical value using a conversion index based on the fluorescence-color scale provided by PAM software. All Fm values below 0.048 were considered invalid to avoid noise bias during imaging-PAM measurements. Indeed, below this threshold, the values acquired were too weak to be reliable (see device manual from Walz, Germany). The quantum efficiency of PSII charge separation (ΔF/Fm') was calculated for each pixel in each image. Subsequently, for each pixel and each actinic light intensity (E; µmol photons $m^{-2}$ $s^{-1}$), the relative electron transport rate was estimated (rETR = ΔF/Fm' x E) and rapid light curves (i.e. rETR vs E curves; RLC) were produced.

*Estimation of photosynthetic parameters.* In order to access the photosynthetic parameters for each pixel of each image, a nonlinear regression model was fitted on the RLC curves using the simplex method of Nelder and Mead (1965). According to the curve profile, the fitting model was automatically chosen by a Matlab© algorithm between that of Webb *et al.* (1974) and that of Eilers and Peeters (1988) to estimate photosynthetic efficiency (α) and capacity ($rETR_{max}$) in relative units. In the exceptional case when the $rETR_{max}$ value estimated was more than twice higher than the highest measured rETR, a linear model was applied to estimate the slope of the curve corresponding to the photosynthetic efficiency (α), and the highest rETR was considered as $rETR_{max}$ to avoid overestimation errors. In the case where (i) the first rETR value was the highest in the RLC, (ii) RLC values were a zero set, or (iii) the set comprised no more than three positive values, the photosynthetic parameters were considered to be invalid. In the end, results were extracted for each pixel giving data sets of 57,132 values and microscale maps for each fluorescence (Fo, Fm, Fv) and photosynthetic parameters (Fv/Fm, α, and $rETR_{max}$) per experimental unit.

### 2.3.2. Chlorophyll *a* and phaeopigment

To quantify the chlorophyll *a* concentration (chl *a* in µg $gDW^{-1}$) in the top centimeter of the sediment, samples from day 6 were freeze-dried and a fraction of about 1 g was weighed for each replicate. Photosynthetic pigments were extracted in 10 ml of 90% acetone at 4 °C for 18 h in the dark under continuous mixing in a rotary shaker. After centrifugation (4 °C, 2,000 g, 5 min), the fluorescence of the supernatant was measured using a Turner Trilogy fluorometer (Turner Designs, Sunnyvale, California, USA) before and after acidification (10 µl of HCl, 0.3 M per 1 ml of sample). Chl *a* values (in µg $gDW^{-1}$) and phaeopigment contents

were then calculated using the Lorenzen method (1966). Phaeopigment contents are expressed as a percentage of total pigments by calculating the following ratio: [phaeo content] / ([phaeo content + chl *a* content]) × 100.

### 2.3.3. Exopolysaccharide contents

Directly after sampling, exopolysaccharides (EPS) were extracted from 5 ml of freshly homogenized sediment placed in 15 ml centrifugation tubes with 5 ml of artificial sea water. After one hour of incubation in a rotary shaker, the tubes were centrifuged (3,000 g, 4 °C, 10 min) and the supernatants containing colloidal exopolysaccharides were placed in a new centrifugation tube. The pellet was used to extract bound EPS with 5 ml of artificial seawater and ~1 g of activated cationic resin (Dowex Marathon C, Na+; Sigma-Aldrich). After resuspension and 1 h of incubation in a rotary shaker, the tubes were centrifuged (3,000 g, 4 °C, 10 min) and the supernatants were collected (Pierre et al. 2012). In both fractions, high molecular weight (HMW) EPS and low molecular weight (LMW) EPS were separated by incubating the supernatants in 70% ethanol at - 20 °C for 16 hours. After centrifugation (3,000 g, 4 °C, 10 min), LMW EPS in the supernatant were discarded and HMW EPS in the pellet were dried at 60 °C in a dry bath under airflow for from six to 48 hours. Dried samples were suspended in 3 ml of milliQ water for carbohydrate and protein quantification. Carbohydrate contents were estimated using sulfuric acid and phenol with glucose as standard (Dubois et al. 1956). Protein contents were estimated using the Bradford assay with bovine serum albumin (BSA) as standard (Bradford 1976). Absorption was then read spectrophotometrically on 96-well plates using a FlexStation plate reader (Molecular Devices) at 485 nm for carbohydrates and 590 nm for proteins. Absorbance were then converted into standard equivalent contents (glucose or BSA) using standard calibration curves and expressed in µg $gDW^{-1}$.

## 2.4. Statistical analyses

Shapiro-Wilk normality tests and Bartlett or Levene equal variance tests were performed on Fo and photosynthetic parameters datasets after Box-Cox transformation if required using the r-package MASS. Statistical analyzes were chosen in order to consider replicated values as a block factor (one block = one experimental unit), time as repeated measured ("within-block" factor), and to test the interaction between independent factors (between block factors). Split-plot ANOVA were then performed on R software to analyze both these datasets with macrofauna density or species as the independent factors. In the case of significant differences in the split-plot ANOVA, a Tukey comparison test were performed with the considered factor to discriminate differences.

For parameters measured once at the end of the experiment (EPS, chl *a*, phaeopigments), after testing the normality and equal variance tests previously mentioned, a one-way ANOVA (AOV) followed by a Tukey test were performed (a Kruskal-Wallis test (KT) followed by a pairwise t-test were performed if application conditions were not met). Data were not transformed before analyses.

Microscale maps were obtained using the Matlab© routine while the other figures were obtained using SigmaPlot (Systat software) or R Software.

## 3. Results

### 3.1. Environmental and sedimentary parameters

During diurnal low tide, light intensity at the sediment surface varied between 84 and 149 µmol photons $m^{-2}$ $s^{-1}$, with an average value of of 114 ± 13 µmol photons $m^{-2}$ $s^{-1}$ while during high tide conditions, light intensity was systematically under 7 µmol photons $m^{-2}$ $s^{-1}$. Water salinity remained constant (17 PSU) throughout the experiment, and the mean water temperature was 12.2 ± 1.1 °C. Sediment analyses revealed a mud percentage (i.e. fine particles <63 µm) of 39.5 ± 2.6% (median grain size of 94.3 ± 9.2 µm), a mean water content of 44.6 ± 1.6%, a mean dry bulk density of 1214.8 ± 24.2 kg $m^{-3}$, and a mean volumetric mass of 1.62 ± 0.1 kg $L^{-1}$.

### 3.2. Chlorophyll *a* biomass and phaeopigments.

Chlorophyll *a* content in control treatments (3.31 ± 0.74 µg chl *a* $gDW^{-1}$) were significantly higher than in *H. diversicolor* (2.30 ± 0.57 µg chl *a* $gDW^{-1}$) and *S. plana* treatments (1.51 ± 0.54 µg chl *a* $gDW^{-1}$) (KT; p-values < 0.001 in both cases). No significant differences were observed between densities of *H. diversicolor* (KT; p-value = 0.14). Conversely, a significant decrease (AOV; p-value < 0.05) in chl *a* content was observed with increasing densities of *S. plana* ranging from 1.8 ± 0.6 to 1.1 ± 0.5 µg chl *a* $gDW^{-1}$ respectively for 249 and 498 ind $m^{-2}$ (fig.1-A).

Phaeopigment percentages in control treatments (74.12 ± 1.63%) were significantly lower than in *H. diversicolor* (80.23 ± 2.55%), and *S. plana* treatments (85.61 ± 2.87%) (KT; p-values < 0.001 in both cases). No significant differences (KT; p-values > 0.05) were observed between the different densities of the two species (fig.1-B).

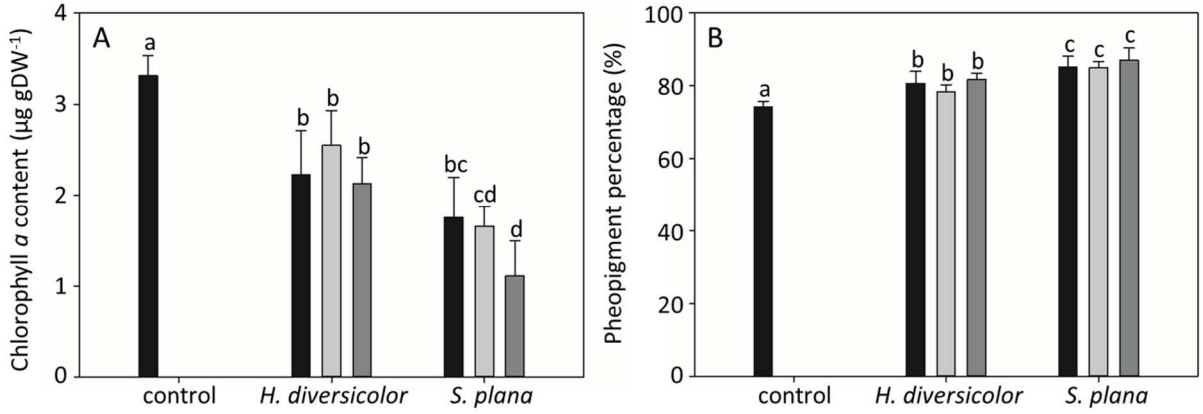


**Figure 1. Variation in A: Chlorophyll a content (chl *a*; µg $gDW^{-1}$) and B: phaeopigment percentage in the top centimeter between treatments.** For treatments with macrofauna, the black bar represents the low density (249 ind $m^{-2}$ for both species), the light grey bar represents the intermediate density (498 and 338 ind $m^{-2}$ for *H. diversicolor* and *S. plana*, respectively) and the dark grey bar represents the high density (747 and 498 ind $m^{-2}$ for *H. diversicolor* and *S. plana*, respectively).

### 3.3. Photosynthetic parameters

*Minimal level of fluorescence as a proxy for photosynthetic biomass*

Imaging-PAM enabled observation of the spatially heterogeneous distribution of fluorescence at the surface of each experimental unit (fig. 2-A). To illustrate changes in spatial distribution of microphytobenthic biofilm on the sediment surface, minimal level of

fluorescence (Fo; unitless) images obtained for each treatment, replicate and daily measurements are provided in Annex. Application of the Matlab© routine allowed to provide a numerical value for each pixel of the analyzed images and thus microscale maps (see example in fig. 2-B). In the example presented in fig. 2, the spatial heterogeneity is high, with a high Fo (up to 0.388) in the lower left side (in red) and a low Fo (up to 0.012) in the upper right side (in blue). The average Fo for the entire surface (n = 57132 pixels) was 0.186.

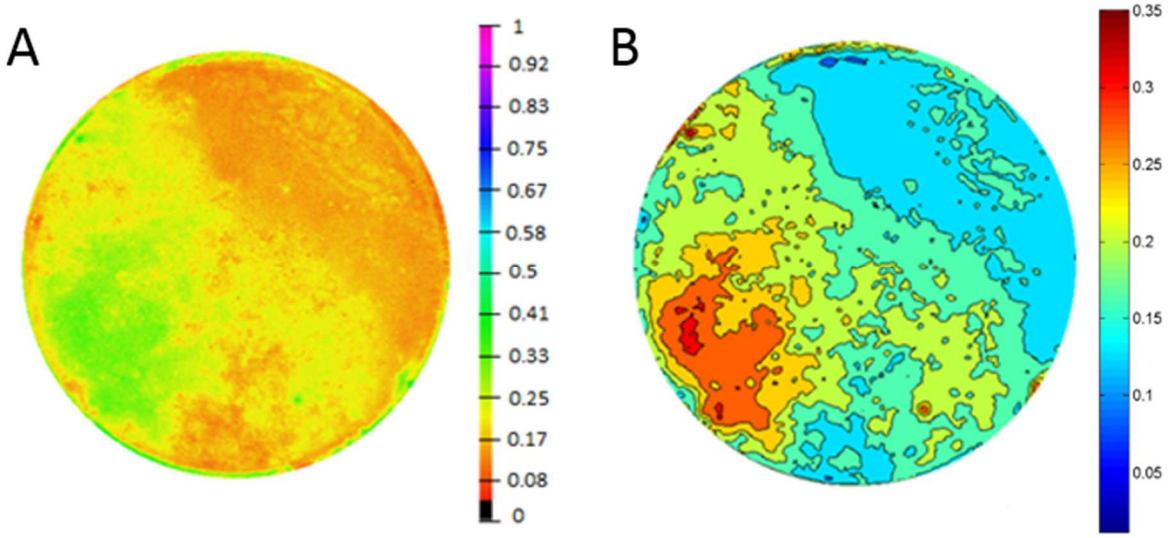


**Figure 2. Microscale spatial map of the minimal level of fluorescence (control treatment, replicate 3, day 6).** With **A:** minimal level of fluorescence (Fo) obtained using imaging-PAM measurement, and **B:** Microscale map with Fo values estimated from image A using the Matlab© routine.

In order to illustrate this spatial variation in microphytobenthic biomass between treatments, the Fo datasets obtained after application of the Matlab© routine on Imaging-PAM images were organized in 5 classes pooling the replicates together (n = 3) for each treatment and each day. All Fo values being ranged between 0.01 and 0.57, Fo < 0.1 were then considered representative of low biomass, and Fo > 0.35 representative of a high biomass. Three classes were defined between these bounds with an amplitude of 0.08. The proportions of each class (%) were calculated and presented in a histogram (fig. 3).

Fo values in the control treatment reached 0.35, but most values were lower than 0.18 (fig. 3-A). A significant increase in Fo values was observed over the course of the experiment (split-plot ANOVA; $F_{df=5;20}$ = 18.08; p-value < 0.001) and the proportion occupied by low Fo values was progressively offset by an increase in the proportion occupied by high Fo values. Indeed, after day 1, 90% of the sediment surface was represented by values < 0.1 while after day 6, approximatively 10% was represented by values between 0.26 and 0.35, 40% between 0.18 and 0.26, 40% between 0.10 and 0.18 and only 10% were < 0.1.

In the presence of *H. diversicolor*, each density followed the same trend than the control treatment and no significant differences were observed between Fo datasets (split-plot ANOVA $F_{df=3;40}$ = 0.13, p-value = 0.94). However, Fo values were above 0.5 with a density of 249 ind $m^{-2}$ (fig. 3-B) and 498 ind $m^{-2}$ (fig. 3-C), and 0.35 for 747 ind $m^{-2}$ (fig. 3-D). In addition, compared to control treatment which presented a maximum value recorded on the 6$^{th}$ day, in presence of *H. diversicolor* the maximum value were recorded on the 5$^{th}$ day for 249

ind $m^{-2}$ and 747 ind $m^{-2}$, and on the 3rd day for 498 ind $m^{-2}$ but with a higher spatial heterogeneity. Indeed, the proportion of sediment with low and high Fo values were both higher in presence of *H. diversicolor* than in control treatments.

In the presence of *S. plana*, each density (fig. 3-E, 3-F, and 3-G) showed significant lower Fo values than in the control treatment (split-plot ANOVA $F_{df=1;50} = 14.99$, p-value < 0.01) with values systematically below 0.16 (maximum value recorded on the 5th day). No significant differences were recorded between Fo datasets of each density (split-plot ANOVA, $F_{df=1;30} = 1.15$, p-value = 0.38).

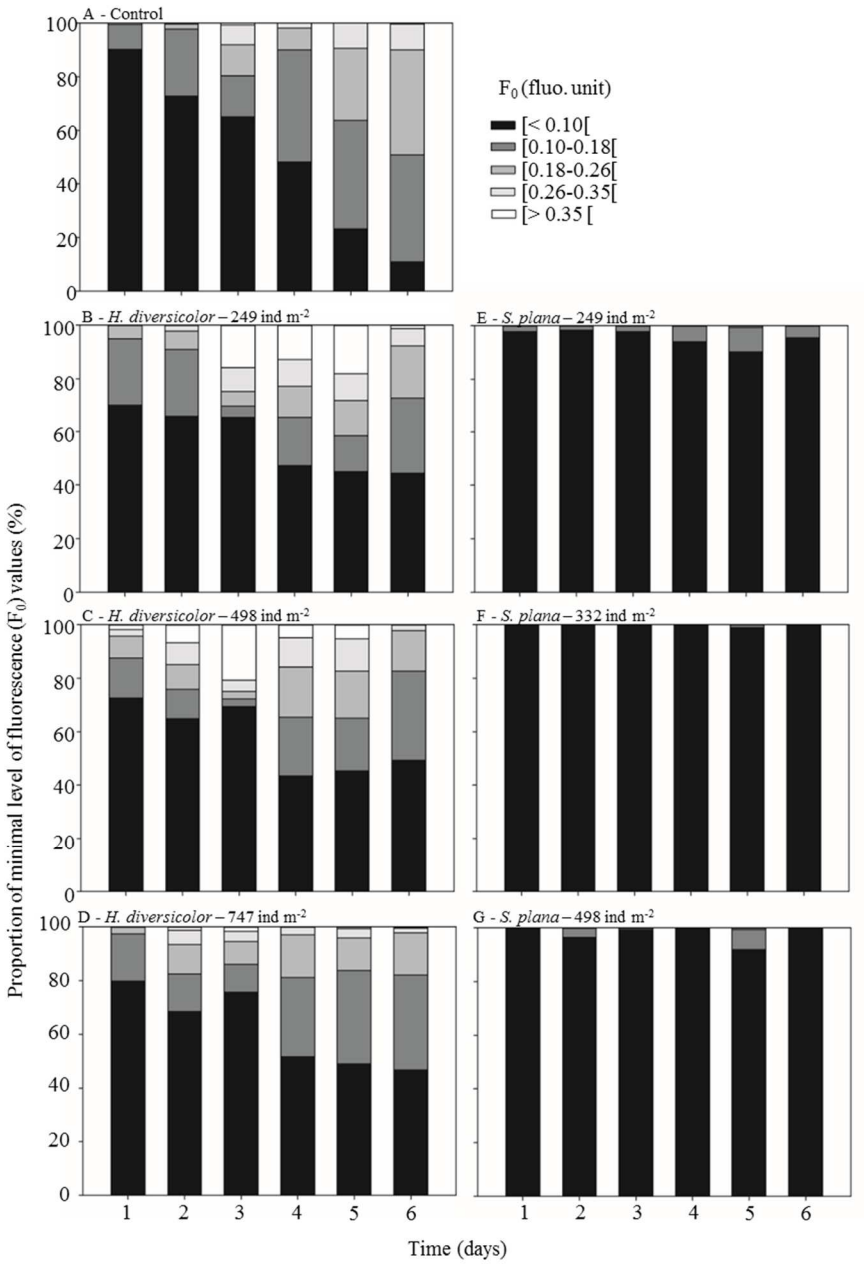


**Figure 3. Heterogeneity of the microphytobenthos biomass using minimal level of fluorescence values (Fo) as a proxy.** The values are presented as a percentage of Fo values belonging to each classis. Proportion of low Fo values in black (<0.1), proportion of high Fo values in white (> 0.35), and according to a gray scale, proportion of Fo values between 0.10 and 0.18 (dark gray), 0.18 and 0.26 (medium gray), and 0.26 and 0.35 (light gray). Each plot represents one treatment: control treatments in A, treatments with *Hediste diversicolor* in B, C, and D (249, 498, and 747 ind $m^{-2}$ respectively), and treatments with *Scrobicularia plana* in E, F, and G (

(249, 332, and 498 ind $m^{-2}$ respectively). Each bar represents one day (from day 1 to day 6) with replicates pooled (n = 3).

*Other photosynthetic parameters*

A marked microscale spatial heterogeneity over the sediment surface of all experimental enclosures was recorded for other photosynthetic parameters, resulting in a high variability both within and between replicates (fig. 4, Annex).

In the control treatment, a significant increase in the number of high values of the maximum quantum efficiency of PSII (Fv/Fm > 0.4) was recorded over the course of the experiment (split-plot ANOVA, $F_{df=5;20} = 4.95$, p-value < 0.01) resulting in an increase in the mean values (fig. 4-A) from day 1 (0.37 ± 0.09) to day 6 (0.50 ± 0.02). In the same way, the mean values of photosynthetic efficiency (α; rel. unit. Fig. 4-B) also increased from day 1 (0.11 ± 0.17) to day 6 (0.34 ± 0.06), and photosynthetic capacity (relative maximum electron transport rate; $rETR_{max}$; rel. unit; fig 4-C) increased from day 1 (22.8 ± 37.2) to day 5 (82.4 ± 18.5).

In the presence of *H. diversicolor*, no significant differences were observed for the photosynthetic parameters between the different densities and with the control treatment (split-plot ANOVAs; p-values > 0.05, fig. 4). Over the course of the experiment, similar mean values (from day 1 to day 6) were measured for Fv/Fm (0.45 ± 0.07 for 249 ind $m^{-2}$, 0.41± 0.09 for 498 ind $m^{-2}$, and 0.39 ± 0.12 for 747 ind $m^{-2}$; Fig. 4-D) and α (0.23 ± 0.09 for 249 ind $m^{-2}$, 0.21 ± 0.13 for 498 ind $m^{-2}$, and 0.20 ± 0.14 for 747 ind $m^{-2}$; Fig. 4-E). However, significantly higher mean values for $rETR_{max}$ were recorded in presence of *H. diversicolor* (89.6 ± 59.4 for 249 ind $m^{-2}$, 84.1 ± 65.5 for 498 ind $m^{-2}$, and 84.1 ± 68.6 for 747 ind $m^{-2}$; Fig. 4-F) than in control treatments (split-plot ANOVA; species:time interaction; $F_{df=5;50} = 2.33$, p-value = 0.0563; fig. 4).

In the presence of *S. plana*, the photosynthetic parameters values were significantly lower than in the control treatment or in presence of *H. diversicolor* (split-plot ANOVAs; p-values < 0.05). Mean values (from day 1 to day 6) of Fv/Fm were 0.30 ± 0.14 for 249 ind $m^{-2}$, 0.19 ± 0.07 for 332 ind $m^{-2}$ and 0.22 ± 0.14 for 498 ind $m^{-2}$ (Fig. 4-G), mean α values were 0.11 ± 0.11 for 249 ind $m^{-2}$, 0.03 ± 0.03 for 338 ind $m^{-2}$ and 0.06 ± 0.08 for 498 ind $m^{-2}$ (Fig. 4-H), while mean $rETR_{max}$ values were 21.8 ± 21.9 for 249 ind $m^{-2}$, 3.7 ± 4.2 for 338 ind $m^{-2}$ and 10.29 ± 15.3 for 498 ind $m^{-2}$ (Fig. 4-I).

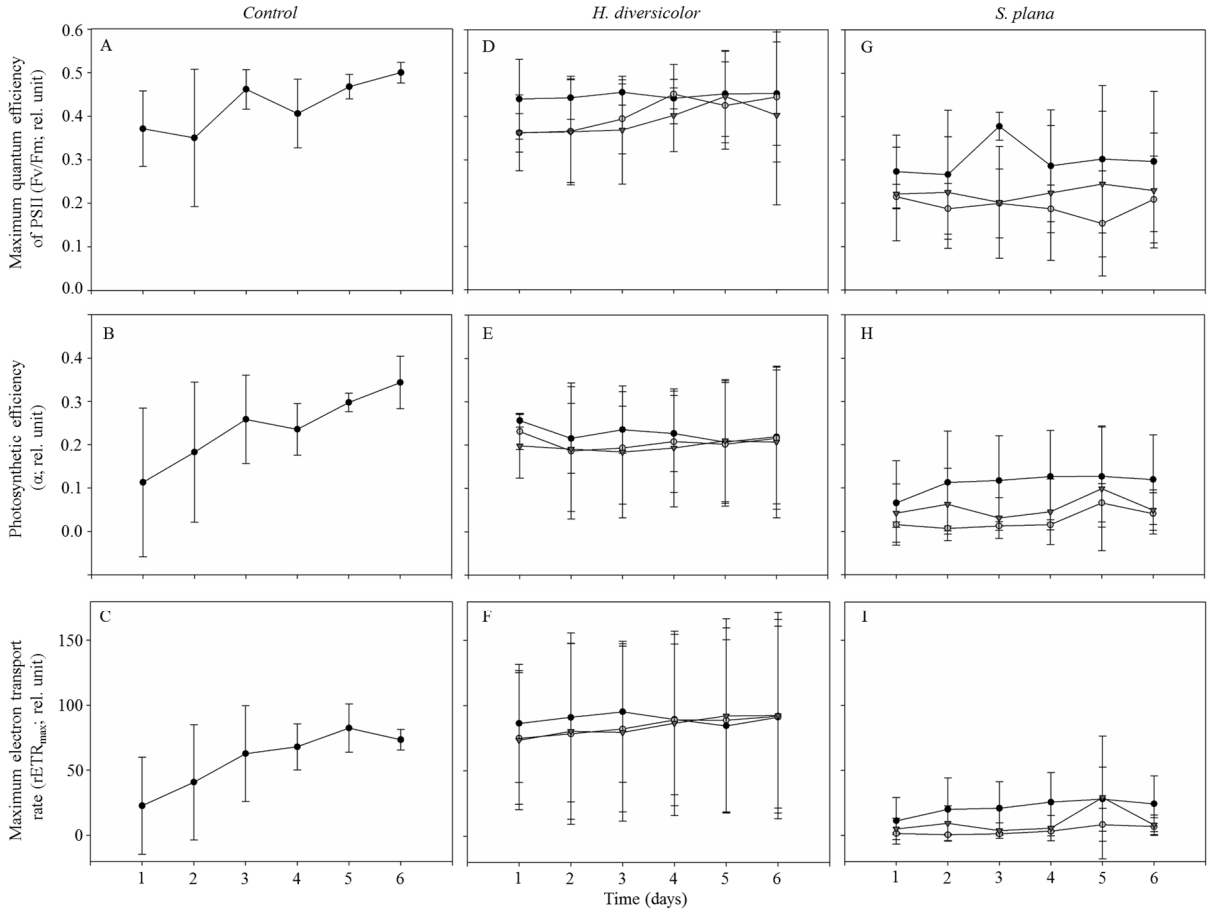


**Figure 4. Variations in mean photosynthetic parameters from day 1 to 6.** With Maximum quantum efficiency of PSII (Fv/Fm; rel. unit), photosynthetic efficiency (α; rel. unit), and maximum electron transport rate ($rETR_{max}$; rel. unit). With control treatment (left panel), treatments with *H. diversicolor* (middle panel) and treatments of *S. plana* (right panel). The gray scale was used to distinguish the different densities of macrofauna with the lowest in black circles (249 ind $m^{-2}$), the middle one in gray circle (498 ind $m^{-2}$ for *H diversicolor* and 332 ind $m^{-2}$ for *S. plana*), and the highest in gray triangle (747 ind $m^{-2}$ for *H diversicolor* and 498 ind $m^{-2}$ for *S. plana*). Mean values were calculated by grouping the values of the replicated enclosure units (n = 3) since the interval between values were similar both within a replicate and between replicates.

### 3.4. Polysaccharides contents

No significant differences were observed between polysaccharides (PS) contents in the different units between treatments (p-values > 0.05). On average, the samples contained 97.7 ± 11.1 µg $gDW^{-1}$ of carbohydrates (Fig. 5-A) and 8.1 ± 2.2 µg $gDW^{-1}$ of proteins (Fig. 5-B). From the total amount of extracted carbohydrates, 72% were external (30% colloidal and 42% bound EPS) while 28% were internal or residual. From extracted proteins, 89% were external (29% colloidal and 60% bound EPS) while 11% were internal or residual.

The polysaccharides concentration per unit of chl *a* in the first centimeter was the lowest in the control treatment with 28.4 ± 3.1 µg PS µg chl $a^{-1}$ for carbohydrates (Fig. 5-C) and 2.0 ± 0.7 µg PS µg chl $a^{-1}$ for proteins (Fig. 5-D). Nevertheless, no significant differences were observed between *H. diversicolor* treatments (in mean 49.3 ± 14.9 µg PS µg chl $a^{-1}$ for carbohydrates and 4.2 ± 1.6 µg PS µg chl $a^{-1}$ for proteins) and control (KT; p- values = 0.16 and 0.05 respectively for carbohydrates and proteins). Densities of *H. diversicolor* showed no effect (KT; p- values = 0.31 and 0.67 respectively for carbohydrates and proteins). In contrast, with *S. plana*, the highest densities showed significant (KT; p-values < 0.05) higher values

(106.9 ± 44.8 µg PS µg chl $a^{-1}$ for carbohydrates and 8.9 ± 3.0 µg PS µg chl $a^{-1}$ for proteins; fig. 5).

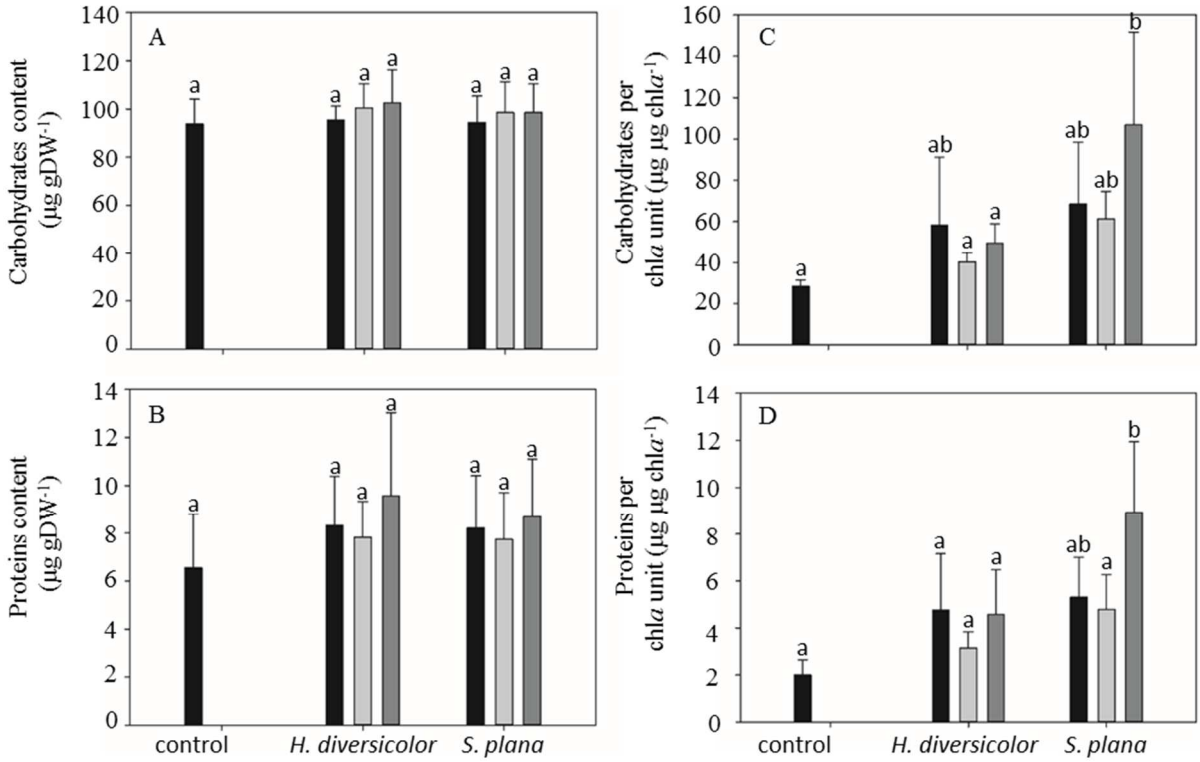


**Figure 5. Carbohydrate and protein contents (µg PS gDW $^{-1}$) in the top centimeter and per unit of chlorophyll *a* (µg PS µg chl *a* $^{-1}$).** For treatments with macrofauna, the black bars represent low density (i.e., 249 ind $m^{-2}$ in both species), the light grey bars represent intermediate density (i.e., 498 and 338 ind $m^{-2}$ for *H. diversicolor* and *S. plana*, respectively) and the dark grey bars represent high density (i.e., 747 and 498 ind $m^{-2}$ for *H. diversicolor* and *S. plana*, respectively).

## 4. Discussion

*Impact of macrofauna on microphytobenthos dynamics*

As hypothesized, the results of this study showed that the presence of the two macrofaunal species, *H. diversicolor* and *S. plana*, had significant effects on microphytobenthic biomass (chl *a*, Fo, phaeopigments). These effects were not straightforward since some non-linear density-dependent functions were obtained. However, some other parameters like EPS concentrations or photosynthetic activity indices showed only few variations related to the macrofaunal density.

In the presence of the benthic tellinid *S. plana*, the microphytobenthic biomass (as illustrated by chl *a* content and Fo) remained lower than in the control treatment during the entire duration of the experiment. This result, combined with the high proportion of phaeopigments, suggests an intense grazing activity (Cartaxana et al. 2003; Orvain et al. 2014b). During emersion periods, this primarily deposit-feeding bivalve continuously ingests large volumes of surficial sediment with their inhalant siphon, leaving star-shaped marks around their burrow opening. Knowing that the siphon can be extended up to 8 cm (Hughes

1969), a single organism can cover a surface area of 201 $cm^2$. Our experimental units had a surface of 68 $cm^2$, allowing a single individual to feed on the entire surface. Even at the lowest tested density (249 ind $m^{-2}$), bivalves deposit-feeding activity can thus drastically limit MPB growth over the entire surface and could explain the weak negative density-dependent effect. In addition, lower values of photosynthetic parameters recorded in the presence of *S. plana* cannot be related to light exposure since all treatment were subject to the same artificial photon flux. Therefore, it seems that, in the presence of *S. plana*, unicellular benthic primary producers were not in optimal conditions to perform photosynthesis. This could be a consequence of biofilm disturbances resulting from sediment reworking linked to feeding and locomotion activities. These latter undoubtedly limited installation and establishment of a stratified biofilm which is a prerequisite for optimal photosynthetic efficiency (Morelle et al. 2020) and thus could explain the lower values of photosynthetic parameters. Moreover, this assumption is supported by the high EPS concentration per unit of chl *a* recorded in the treatment with the highest density of *S. plana*. Indeed, it would first illustrate the consequence of intense cell lysis induced by consumption of the biofilm, which would be consistent with the values of phaeopigments and especially the proteins concentration since protein excretion is very costly for microphytobenthic cells. Second, the EPS excretion by microphytobenthic cells could reflect the construction of new biofilms and/or the vertical migration after sediment reworking. Especially carbohydrate EPS which are known to play a role in the movement of epipelic benthic diatoms and allows cells to adhere to sediment surfaces (Perkins et al. 2001; Orvain et al. 2003; Tolhurst et al. 2003; De Brouwer et al. 2006; Shnyukova and Zolotareva 2017) especially in pioneering stages (Gerbersdorf et al. 2009; Lubarsky et al. 2010; Orvain et al. 2014a).

The strong influence of *S. plana* on MPB biomass and photosynthetic capacity observed in this study is inquiring. Indeed, because of winter conditions, definitely not optimal for this species which prefers temperature between 24 and 30 °C, its feeding activity was probably reduced (Hughes 1969). This shows that deposit-feeding bivalves are able to quickly limit MPB growth, even at low density and under sub-optimal conditions. S. *plana* being widely distributed in estuarine mudflats, sometimes in very high densities (Santos et al. 2011), it undoubtedly plays a key role in the control of MPB primary production and could in turn impact the trophic network and the stability of the sediment surface. These results suggest that, regardless of environmental conditions, performing photosynthesis in ecosystems colonized by *S. plana* would be very difficult for microphytobenthic species, in the range of density tested. This is in accordance with the drastic effect of *S. plana* on MPB biomass also observed in the same range of density in Marennes-Oléron Bay (Orvain et al. 2007). However, it is highly probable that non-lethal predation of *S. plana* which is a common prey for birds (waders, gulls) and fish, resulting in the strong reduction of siphon extension and feeding activity (Maire et al. 2010), profoundly limit this negative impact on microbenthic primary production. Therefore, the trophic chain associating MPB and *S. plana* would to be regulated by a top-down cascade involving the regulation of lower trophic compartments by the higher ones (Sommer and Stibor 2002; Caraco *et al.* 2006; Sommer and Sommer 2006). Moreover, this observe top-down regulation of MPB by macrofauna must also induce cascade effects regarding sediment 3D structure since fauna/MPB interaction can control the bed elevation and its micro-heterogeneity (Weerman et al. 2011).

In the presence of the polychaete *H. diversicolor*, results were more subject to fluctuations and the density-dependent relationship was more complex. Despite the higher proportion of surface area with a low MPB biomass than in the control treatment, there was also a higher proportion of surface area with a high MPB biomass. The high proportion of surface area with a low MPB biomass combined with the high phaeopigment proportion confirmed that part of the MPB biomass was consumed by grazing activity (Cartaxana et al. 2003; Orvain et al. 2014b). Indeed, *H. diversicolor* is an omnivorous predator (Costa *et al.* 2006) that largely consumes microphytobenthic biofilm at the sediment surface (Passarelli et al. 2012). During high tide, *H. diversicolor* can behave as a filter-feeder using a secreted mucous filter that traps particles (Riisgard 1991; Scaps 2002) while during low tide, two feeding strategies are observed. The first one consists in crawling on the sediment surface prospecting for food, and the second one in trapping food in a mucous secretion (Esselink and Zwarts 1989; Esnault *et al.* 1990; Scaps 2002). These feeding behaviors, especially during low tide, could explain the observed disappearance of photosynthetic cells over a portion of the surface area (around 20-30% of the experimental unit surface) compared with control treatments. However, in contrast to *S. plana*, the presence of *H. diversicolor* did not appear to limit biofilm growth and the physiological state of microphytobenthic cells illustrated by the Fo dataset and the Fv/Fm values which were not different than in the control treatment. The values of $rETR_{max}$ higher in the presence of *H. diversicolor* than in the control even seem to indicate that the photosynthetically active cells were more efficient. Reinforced by the fact that the highest values of photosynthetic parameters were reached more quickly in presence of *H. diversicolor* than in the control, these results may even suggest that the presence of *H. diversicolor* could promote MPB growth (Kristensen 1993; Tang and Kristensen 2007; Passarelli et al. 2012). Although direct measurements of nutrient fluxes are lacking, these results could be explained by the effect of *H. diversicolor* on nutrient diffusion in the sediment surface *via* its bioirrigation effects (Mermillod-Blondin et al. 2004; Volkenborn et al. 2016), as also assumed for other bioturbators like the nematodes (D'Hondt et al. 2018), the bivalve *Cerastoderma edule* (Swanberg 1991; Donadi et al. 2015), or the annelid worm *Arenicola marina* (Chennu et al. 2015; Eriksson et al. 2017). Indeed, frequent ventilation of galleries enhances bacterial productivity and nutrient fluxes across the sediment-water interface, and bioirrigation rates by *H. diversicolor* are positively correlated with densities (Davey and Watson 1995). The vertical upward fluxes of nutrients caused by bioirrigation along the galleries could thus increase the access to nutrients for MPB and enables protein synthesis that is crucial to maintain growth, avoid alteration of photosynthetic capacities, and reconstitute pioneering biofilms (Orvain et al. 2014a). This could therefore explain the higher proportion of area with a high biomass. However, the potential positive effect of bioirrigation by *H. diversicolor* on nutrient fluxes (Kristensen and Hansen 1999) and especially on microphytobenthic growth and photosynthetic activity remains difficult to established since this process is always associated with a parallel grazing effect (Passarelli et al. 2012), deleting the positive influence of bioturbation. This could explain the absence of differences observed between the treatments of *H. diversicolor* and the control ones. Nevertheless, there are good proxies exhibiting that the grazing pressure is balanced by positive effects of this deposit-feeding annelid.

In parallel, the absence of differences observed between the different densities could be explained by the influence of density on feeding behavior (Duport et al. 2006). As also observed for closely related species like the annelid worm *Alitta virens* which exhibits comparable lifestyles and feeding behaviors, individual prospecting rates could have decreased (Miron *et al.* 1991) and/or individual food prospecting areas could be reduced when individuals density increase in order to share the trophic resource (Esnault et al. 1990). However, a time lag was observed between densities when the proportion of high Fo values decrease after several days. This observation suggests that, the modification of the feeding behavior at high density and the compensation process between grazing and enhancement of nutrient fluxes could have a limit in time which must depend on the range of the worm density and body size. Nevertheless, being able to tolerate major variations in temperature and salinity (Wolff 1973), *H. diversicolor* individuals were in optimal conditions and their feeding behavior may have been more active than it would be in natural environmental conditions. In addition, *H. diversicolor* is a common prey for numerous predators inhabiting intertidal mudflats, especially birds (waders and shelducks) which may consume up to 90% of a population (Evans *et al.* 1979).

*Microscale spatial heterogeneity of microphytobenthos*

A strong variability between replicates was observed in this study for Fo and photosynthetic parameters and could be attributed to the time lag between measurements due to migration of microphytobenthic cells along the photoperiod (Barnett et al. 2020). However, the intra-unit microscale heterogeneity observed was as important as the inter-unit one and highlights the strong patchiness of MPB biomass at microscale. The difference of the heterogeneity level between treatments (i.e., lower in control units than in presence of bioturbators), confirms the importance of the external forcing on this patchiness like the biological activity but also other physical factors directly impacting sediment topography (e.g. water flows on the sediment surface). This observation confirms that the strong micro-scale heterogeneity in MPB distribution makes particularly difficult to accurately estimate spatial dynamics of MPB (1) biomass (Seuront and Spilmont 2002) and (2) photosynthetic parameters at larger spatial scales when based on one-shot measurements (Kromkamp et al. 2020). As widely shown in the literature, fluorescence measurements performed with pulse amplitude modulated (PAM) fluorometer is a very useful tool in microphytobenthic photosynthesis studies (Underwood and Kromkamp 1999). However, the use of fluorescence values obtained without taking this spatial heterogeneity into consideration may significantly influence the reliability of estimated photosynthetic parameters at larger scale and could lead to significant over- or under-estimations. Consequently, the spatial heterogeneity of fluorescence should be systematically considered when photosynthetic parameters are estimated at larger scale using the PAM method. This could be achieved, for instance, by performing numerous replicates in a given environment as proposed by Spilmont et al. (2011) for chlorophyll *a* or as performed using a PAM fluorometer by Kromkamp et al. (2020).

However, caution is still required as imaging-PAM measurements are restricted to the top millimeters of the chlorophyll profile (Vieira et al. 2013a). Indeed, light and fluorescence attenuation are mainly dependent of MPB vertical distribution, its migratory behavior and the

sediment granulometry (Kühl and Jørgensen 1994; Forster and Kromkamp 2004; Serôdio 2004; Frankenbach and Serôdio 2017). Yet, chl *a* profiles illustrate that as a function of the biofilm structuration, chl *a* content in the top first millimeters can easily be under 10% of the total active chl *a* in the top first centimeter (Méléder et al. 2005; Jesus et al. 2006; Lake and Brush 2011; Frankenbach et al. 2019; Morelle et al. 2020). Therefore, for further users of Imaging-PAM fluorometer, we warmly recommend the parallel use of a correction tool integrating the chl *a* distribution profiles (Forster and Kromkamp 2004; Serôdio 2004; Vieira et al. 2013b; Morelle et al. 2018a). Another alternative to avoid a potential bias in fluorescence estimation would be to use the imaging-PAM fluorometer to capture images of the spatial microscale heterogeneity of fluorescence vertically with depth. This could be assessed by cutting vertically an experimental unit but it would be necessary to not disturb the matrix, maybe by using cryolanding techniques (Paterson 1989; De Brouwer and Stal 2001; Kelly et al. 2001; Laviale et al. 2015). Coupling fluorescence estimates with depth and on the surface at such spatial microscale heterogeneity could allowed to estimate photosynthetic parameters more accurately than ever before.

*Conclusion*

On one hand, the present study showed that nutrition and bioturbation activity, mainly sediment reworking, performed by *S. plana* seems to strongly limit MPB growth and photosynthetic capacities. This negative effect would be even higher in summer when conditions are more favorable for both macrofaunal species and microbial communities. On another hand, our results showed a potential effect of *H. diversicolor* on nutrient diffusion on the sediment surface *via* its bioirrigation activity that could enhance microphytobenthic growth and offset biomass losses through nutrition. It is now necessary to further investigate the vertical fluxes of nutrients and bioturbation-related transport rates within the sediment matrix to confirm this hypothesis. In both cases, predation of these two species would play a major role in the regulation of lower trophic compartments up to the microphytobenthic one trough a top-down cascade. This study also supports the importance to consider the microscale spatial heterogeneity of the microphytobenthic biofilm and further suggest to consider the coupling with depth profiles at the same micro-scale to improve estimates.

**Credit Author Statement**

**Jérôme Morelle:** Investigation, Formal analysis, Writing - Original Draft**. Olivier Maire:** Methodology, Resources, Investigation, Writing - Review & Editing. **Anaïs Richard:** Investigation, Formal analysis. **Alex Slimani:** Investigation, Software. **Francis Orvain:** Funding acquisition, Methodology, Resources, Investigation, Software, Writing - Review & Editing

**Acknowledgments**

The authors wish to thank those who participated in the sampling and treatments especially Thomas Lecarpentier, Edith Parlanti, Mahaut Sourzac and Arnaud Huguet. We also thank Anniet Laverman and Pascal Claquin for the constructive comments and discussions. We are grateful to the ASLO 2019 Aquatic Sciences Meeting in Puerto Rico which allowed us to

communicate on this study during the event. We also thank the GIP Seine-Aval and especially Nicolas Bacq for his implication in the PHARE-SEE project.

## References

An, S., and S. B. Joye. 2001. Enhancement of coupled nitrification-denitrification by benthic photosynthesis in shallow estuarine sediments. Limnol. Oceanogr. **46**: 62–74.

Barnett, A., V. Méléder, C. Dupuy, and J. Lavaud. 2020. The Vertical Migratory Rhythm of Intertidal Microphytobenthos in Sediment Depends on the Light Photoperiod, Intensity, and Spectrum: Evidence for a Positive Effect of Blue Wavelengths. Frontiers in Marine Science **7**: 1–18.

Bergayou, H., E. M. Anajjar, L. Lefrère, A. Moukrim, and P. Gillet. 2019. Recovery of an estuarine ecosystem after the stopping of wastewater discharge: Intertidal macrobenthic community characterization in the estuary of oued souss (Southwestern Morocco). Journal of Ecological Engineering **20**: 133–145.

Blanchard, G. F., J.-M. Guarini, P. Richard, P. Gros, and F. Mornet. 1996. Quantifying the short-term temperature effect on light-saturated photosynthesis of intertidal microphytobenthos. Marine Ecology Progress Series **134**: 309–313.

Bradford, M. M. 1976. A rapid and sensitive method for the quantitation of microgram quantities of protein utilizing the principle of protein-dye binding. Analytical biochemistry **72**: 248–254.

Braeckman, U., P. Provoost, B. Gribsholt, D. Van Gansbeke, J. J. Middelburg, K. Soetaert, M. Vincx, and J. Vanaverbeke. 2010. Role of macrofauna functional traits and density in biogeochemical fluxes and bioturbation. Marine Ecology Progress Series **399**: 173–186.

De Brouwer, J. F. C., T. R. Neu, and L. J. Stal. 2006. On the function of secretion of extracellular polymeric substances by benthic diatoms and their role in intertidal mudflats: A review of recent insights and views, p. 45–61. *In* J.C. Kromkamp, J.F.C. De Brouwer, G.F. Blanchard, R.M. Forster, and V. Créac [eds.], Functioning of microphytobenthos in estuaries. Royal Netherlands Academy of Arts and Sciences.

De Brouwer, J. F. C., and L. J. Stal. 2001. Short-term dynamics in microphytobenthos distribution and associated extracellular carbohydrates in surface sediments of an intertidal mudflat. Marine Ecology Progress Series **218**: 33–44.

Caraco, N. F., J. J. Cole, and D. L. Strayer. 2006. Top down control from the bottom: Regulation of eutrophication in a large river by benthic grazing. Limnology and Oceanography **51**: 664–670.

Cartaxana, P., N. Domingues, S. Cruz, B. Jesus, M. Laviale, J. Serôdio, and J. M. Da Silva. 2013. Photoinhibition in benthic diatom assemblages under light stress. Aquatic Microbial Ecology **70**: 87–92.

Cartaxana, P., B. Jesus, and V. Brotas. 2003. Pheophorbide and pheophytin a-like pigments as useful markers for intertidal microphytobenthos grazing by Hydrobia ulvae. Estuarine, Coastal and Shelf Science **58**: 293–297.

Cartaxana, P., L. Ribeiro, J. W. Goessling, S. Cruz, and M. Kühl. 2016. Light and O<>2<> microenvironments in two contrasting diatom-dominated coastal sediments. Marine Ecology Progress Series **545**: 35–47.

Chennu, A., N. Volkenborn, D. De Beer, D. S. Wethey, S. A. Woodin, and L. Polerecky. 2015. Effects of bioadvection by Arenicola marina on microphytobenthos in permeable sediments. PLoS ONE **10**: 1–16.

Costa, P. F. E., R. F. Oliveira, and L. C. Da Fonseca. 2006. Feeding Ecology of Nereis diversicolor (O. F. Müller) (Annelida, Polychaeta) on Estuarine and Lagoon

Environments in the Southwest Coast of Portugal. Pan-American Journal of Aquatic Sciences **1**: 114–126.

D'Hondt, A. S., W. Stock, L. Blommaert, T. Moens, and K. Sabbe. 2018. Nematodes stimulate biomass accumulation in a multispecies diatom biofilm. Marine Environmental Research **140**: 78–89.

Dauvin, J. C., and N. Desroy. 2005. The food web in the lower part of the Seine estuary: A synthesis of existing knowledge. Hydrobiologia **540**: 13–27.

Davey, J. T., and P. G. Watson. 1995. The activity of Nereis Diversicolor (Polychaeta) and its impact on nutrient fluxes in estuarine waters AU - Davey, J. T. Ophelia **41**: 57–70.

Donadi, S., T. van der Heide, T. Piersma, E. M. van der Zee, E. J. Weerman, J. van de Koppel, H. Olff, C. Devine, U. E. Hernawan, M. Boers, L. Planthof, and B. Klemens Eriksson. 2015. Multi-scale habitat modification by coexisting ecosystem engineers drives spatial separation of macrobenthic functional groups. Oikos **124**: 1502–1510.

Donadi, S., J. Westra, E. J. Weerman, T. Van Der Heide, E. M. Van Der Zee, J. Van De Koppel, H. Olff, H. W. Van Der Veer, and B. Klemens Eriksson. 2013. Non-trophic Interactions Control Benthic Producers on Intertidal Flats. Ecosystems **16**: 1325–1335.

Dubois, M., K. A. Gilles, J. K. Hamilton, Pa. Rebers, and F. Smith. 1956. Colorimetric method for determination of sugars and related substances. Analytical chemistry **28**: 350–356.

Duport, E., G. Stora, P. Tremblay, and F. Gilbert. 2006. Effects of population density on the sediment mixing induced by the gallery-diffusor Hediste (Nereis) diversicolor O.F. Müller, 1776. Journal of Experimental Marine Biology and Ecology **336**: 33–41.

Eilers, P. H. C., and J. C. H. Peeters. 1988. A model for the relationship between light intensity and the rate of photosynthesis in phytoplankton. Ecological Modelling **42**: 199–215.

Eriksson, B. K., J. Westra, I. Van Gerwen, E. J. Weerman, E. Vander Zee, T. Vander Heide, J. Vande Koppel, H. Olff, T. Piersma, and S. Donadi. 2017. Facilitation by ecosystem engineers enhances nutrient effects in an intertidal system. Ecosphere **8**, doi:10.1002/ecs2.2051

Esnault, G., C. Retiere, and R. Lambert. 1990. Food resource partitioning in a population of Nereis diversicolor (Annelida, Polychaeta) under experimental conditions. Trophic Relationships in the Marine Environment **453467**: 453–467.

Esselink, P., and L. Zwarts. 1989. Seasonal trend in burrow depth and tidal variation in feeding activity of Nereis diversicolor. Marine Ecology Progress Series **56**: 243–254.

Evans, P. R., D. M. Herdson, P. J. Knights, and M. W. Pienkowski. 1979. Short-term effects of reclamation of part of Seal Sands, Teesmouth, on wintering waders and Shelduck. Oecologia **41**: 183–206.

Forster, R. M., and J. C. Kromkamp. 2004. Modelling the effects of chlorophyll fluorescence from subsurface layers on photosynthetic efficiency measurements in microphytobenthic algae. Marine Ecology Progress Series **284**: 9–22.

Frankenbach, S., A. A. Azevedo, V. Reis, D. Dias, L. Vaz, J. M. Dias, and J. Serôdio. 2019. Functional resilience of PSII, vertical distribution and ecosystem-level estimates of subsurface microphytobenthos in estuarine tidal flats. Continental Shelf Research **182**: 46–56.

Frankenbach, S., and J. Serôdio. 2017. One pulse, one light curve: Fast characterization of the light response of microphytobenthos biofilms using chlorophyll fluorescence. Limnology and Oceanography: Methods **15**: 554–566.

Froelich, P. N., G. P. Klinkhammer, M. L. Bender, N. A. Luedtke, G. R. Heath, D. Cullen, P. Dauphin, D. Hammond, B. Hartman, and V. Maynard. 1979. Early ocidation of organic matter in pelagic sediments of the eastern equatorial Atlantic: suboxic diagenesis.

Geochimica et Cosmochimica Acta **43**: 1075–1090.
Gerbersdorf, S. U., R. Bittner, H. Lubarsky, W. Manz, and D. M. Paterson. 2009. Microbial assemblages as ecosystem engineers of sediment stability. J soils Sediments **9**: 640–652.
Guarini, J.-M., G. F. Blanchard, and P. Gros. 2000. Quantification of the microphytobenthic primary production in European intertidal mudflats – a modelling approach. Continental Shelf Research **20**: 1771–1788.
Henrichs, S. M. 1992. Early diagenesis of organic matter in marine sediments: progress and perplexity. Marine Chemistry **39**: 119–149.
Hochard, S., C. Pinazo, C. Grenz, J. L. B. Evans, and O. Pringault. 2010. Impact of microphytobenthos on the sediment biogeochemical cycles: A modeling approach. Ecological Modelling **221**: 1687–1701.
Hope, J. A., D. M. Paterson, and S. F. Thrush. 2020. The role of microphytobenthos in soft-sediment ecological networks and their contribution to the delivery of multiple ecosystem services. Journal of Ecology **108**: 815–830.
Hughes, B. B., M. D. Levey, J. A. Brown, M. C. Fountain, A. B. Carlisle, S. Y. Litvin, C. M. Greene, W. N. Heady, and M. G. Gleason. 2014. Nursery Functions of U.S. West Coast Estuaries: The State of Knowldege for Juveniles of Focal Invertebrate and Fish Species, p. 168. *In* The Nature Conservancy, Arlington, VA.
Hughes, R. N. 1969. A study of feeding in Scrobicularia plana. Journal of the Marine Biological Association of the United Kingdom **49**: 805–823.
Jesus, B., V. Brotas, M. Marani, and D. M. Paterson. 2005. Spatial dynamics of microphytobenthos determined by PAM fluorescence. Estuarine, Coastal and Shelf Science **65**: 30–42.
Jesus, B., V. Brotas, L. Ribeiro, C. R. Mendes, P. Cartaxana, and D. M. Paterson. 2009. Adaptations of microphytobenthos assemblages to sediment type and tidal position. Continental Shelf Research **29**: 1624–1634.
Jesus, B., C. R. Mendes, V. Brotas, and D. M. Paterson. 2006. Effect of sediment type on microphytobenthos vertical distribution: Modelling the productive biomass and improving ground truth measurements. Journal of Experimental Marine Biology and Ecology **332**: 60–74.
Kelly, J. A., C. Honeywill, and D. M. Paterson. 2001. Microscale analysis of chlorophyll-a in cohesive, intertidal sediments: the implications of microphytobenthos distribution. Journal of the Marine Biological Association of the UK **81**: 151–162.
Van Kooten, O., and J. F. H. Snel. 1990. The use of chlorophyll fluoresence nomenclature in plant stress physiology. Photosynthesis Research **25**: 147–150.
Kristensen, E. 1993. Seasonal variations in benthic community metabolism and nitrogen dynamics in a shallow, organic-poor danish lagoon. Estuarine Coastal and Shelf Science **36**: 565–586.
Kristensen, E. 2001. Impact of polychaetes (Nereis spp. and Arenicola marina) on carbon biogeochemistry in coastal marine sediments. Geochemical Transactions **2**: 92–103.
Kristensen, E., J. M. Neto, M. Lundkvist, L. Frederiksen, M. Â. Pardal, T. Valdemarsen, and M. R. Flindt. 2013. Influence of benthic macroinvertebrates on the erodability of estuarine cohesive sediments: Density- and biomass-specific responses. Estuarine, Coastal and Shelf Science **134**: 80–87.
Kristensen, K., and K. Hansen. 1999. Transport of carbon dioxide and ammonium in bioturbated (Nereis diversicolor) coastal, marine sediments. Biogeochemistry **45**: 147–168.
Kromkamp, J. C., E. Morris, and R. M. Forster. 2020. Microscale Variability in Biomass and Photosynthetic Activity of Microphytobenthos During a Spring-Neap Tidal Cycle. Frontiers in Marine Science **7**: 1–15.

Kromkamp, J., and J. Peene. 1999. Estimation of phytoplankton photosynthesis and nutrient limitation in the Eastern Scheldt estuary using variable fluorescence. Aquatic Ecology **33**: 101–104.

Kühl, M., and B. B. Jørgensen. 1994. The light-field of microbenthic communities- radiance distribution and microscale optics of sandy coastal sediments. Limnology and Oceanography **39**: 1368–1398.

Kuwae, T., P. G. Beninger, P. Decottignies, K. J. Mathot, D. R. Lund, and R. W. Elner. 2008. Biofilm grazing in a higher vertebrate: The western sandpiper, Calidris Mauri. Ecology **89**: 599–606.

Lake, S. J., and M. J. Brush. 2011. The contribution of microphytobenthos to total productivity in upper Narragansett Bay, Rhode Island. Estuarine, Coastal and Shelf Science **95**: 289–297.

Laviale, M., J. Ezequiel, C. Pais, P. Cartaxana, and J. Serôdio. 2015. The "crème brûlée" sampler: A new high-resolution method for the fast vertical sampling of intertidal fine sediments. Journal of Experimental Marine Biology and Ecology **468**: 37–44.

Lohrer, A. M., N. J. Halliday, S. F. Thrush, J. E. Hewitt, and I. F. Rodil. 2010. Ecosystem functioning in a disturbance-recovery context: Contribution of macrofauna to primary production and nutrient release on intertidal sandflats. Journal of Experimental Marine Biology and Ecology **390**: 6–13.

Lorenzen, C. J. 1966. A method for the continuous measurement of in vivo chlorophyll concentration. Deep Sea Research and Oceanographic Abstracts **13**: 223–227.

Lubarsky, H. V, C. Hubas, M. Chocholek, F. Larson, W. Manz, D. M. Paterson, and S. U. Gerbersdorf. 2010. The stabilisation potential of individual and mixed assemblages of natural bacteria and microalgae. PloS one **5**: e13794.

Maire, O., J. N. Merchant, M. Bulling, L. R. Teal, A. Grémare, J. C. Duchêne, and M. Solan. 2010. Indirect effects of non-lethal predation on bivalve activity and sediment reworking. Journal of Experimental Marine Biology and Ecology **395**: 30–36.

Méléder, V., L. Barillé, Y. Rincé, M. Morançais, P. Rosa, and P. Gaudin. 2005. Spatiotemporal changes in microphytobenthos structure analysed by pigment composition in a macrotidal flat (Bourgneuf Bay, France). Marine Ecology Progress Series **297**: 83–99.

Mermillod-Blondin, F., R. Rosenberg, F. François-Carcaillet, K. Norling, and L. Mauclaire. 2004. Influence of bioturbation by three benthic infaunal species on microbial communities and biogeochemical processes in marine sediment. Aquatic Microbial Ecology **36**: 271–284.

Miron, G., G. Desrosiers, C. Retière, and R. Lambert. 1991. Dispersion and prospecting behaviour of the polychaete Nereis virens ( Sars ) as a function of density. Journal of Experimental Marine Biology and Ecology **145**: 65–77.

Morelle, J., P. Claquin, and F. Orvain. 2020. Evidence for better microphytobenthos dynamics in mixed sand/mud zones than in pure sand or mud intertidal flats (Seine estuary, Normandy, France). PloS one **15**: e0237211.

Morelle, J., F. Orvain, and P. Claquin. 2018a. A simple , user friendly tool to readjust raw PAM data from fi eld measurements to avoid over- or underestimating of microphytobenthos photosynthetic parameters. Journal of Experimental Marine Biology and Ecology **503**: 136–146.

Morelle, J., M. Schapira, F. Orvain, P. Riou, P. J. Lopez, O. Pierre-Duplessix, E. Rabiller, F. Maheux, B. Simon, and P. Claquin. 2018b. Annual Phytoplankton Primary Production Estimation in a Temperate Estuary by Coupling PAM and Carbon Incorporation Methods. Estuaries and Coasts **41**, doi:10.1007/s12237-018-0369-8

Nelder, J. A., and R. Mead. 1965. A simplex method for function minimization. The computer

journal **7**: 308–313.

Ní Longphuirt, S., J. H. Lim, A. Leynaert, P. Claquin, E. J. Choy, C. K. Kang, and S. An. 2009. Dissolved inorganic nitrogen uptake by intertidal microphytobenthos: Nutrient concentrations, light availability and migration. Marine Ecology Progress Series **379**: 33–44.

Orvain, F. 2005. A model of sediment transport under the influence of surface bioturbation: Generalisation to the facultative suspension-feeder Scrobicularia plana. Marine Ecology Progress Series **286**: 43–56.

Orvain, F., M. De Crignis, K. Guizien, S. Lefebvre, C. Mallet, E. Takahashi, and C. Dupuy. 2014a. Tidal and seasonal effects on the short-term temporal patterns of bacteria, microphytobenthos and exopolymers in natural intertidal biofilms (Brouage, France). Journal of Sea Research **92**: 6–18.

Orvain, F., R. Galois, C. Barnard, A. Sylvestre, G. Blanchard, and P.-G. Sauriau. 2003. Carbohydrate production in relation to microphytobenthic biofilm development: an integrated approach in a tidal mesocosm. Microbial ecology **45**: 237–251.

Orvain, F., K. Guizien, S. Lefebvre, M. Bréret, and C. Dupuy. 2014b. Relevance of macrozoobenthic grazers to understand the dynamic behaviour of sediment erodibility and microphytobenthos resuspension in sunny summer conditions. Journal of Sea Research **92**: 46–55.

Orvain, F., P. G. Sauriau, A. Sygut, L. Joassard, and P. Le Hir. 2004. Interacting effects of Hydrobia ulvae bioturbation and microphytobenthos on the erodibility of mudflat sediments. Marine Ecology Progress Series **278**: 205–223.

Orvain, F., P. Sauriau, P. Le Hir, G. Guillou, P. Cann, and M. Paillard. 2007. Spatio-temporal variations in intertidal mudflat erodability : Marennes- Oléron Bay , western France. Continental Shelf Research **27**: 1153–1173.

Passarelli, C., C. Hubas, A. N. Segui, J. Grange, and T. Meziane. 2012. Surface adhesion of microphytobenthic biofilms is enhanced under Hediste diversicolor (O.F. Müller) trophic pressure. Journal of Experimental Marine Biology and Ecology **438**: 52–60.

Paterson, D. M. 1989. Short-term changes in the erodibility of intertidal cohesive sediments related to the migratory behavior of epipelic diatoms. Limnol. Oceanogr. **34**: 223–234.

Paterson, D. M., and S. E. Hagerthey. 2001. Microphytobenthos in constrasting coastal ecosystems: biology and dynamics, p. 105–125. *In* Ecological comparisons of sedimentary shores. Springer.

Perkins, R. G., J. Lavaud, J. Serôdio, J. L. Mouget, P. Cartaxana, P. Rosa, L. Barille, V. Brotas, and B. M. Jesus. 2010. Vertical cell movement is a primary response of intertidal benthic biofilms to increasing light dose. Marine Ecology Progress Series **416**: 93–103.

Perkins, R. G., G. J. C. Underwood, V. Brotas, G. C. Snow, B. Jesus, and L. Ribeiro. 2001. Responses of microphytobenthos to light: Primary production and carbohydrate allocation over an emersion period. Marine Ecology Progress Series **223**: 101–112.

Pierre, G., M. Graber, B. A. Rafiliposon, C. Dupuy, F. Orvain, M. de Crignis, and T. Maugard. 2012. Biochemical Composition and Changes of Extracellular Polysaccharides (ECPS) Produced during Microphytobenthic Biofilm Development (Marennes-Oléron, France). Microbial Ecology **63**: 157–169.

Rakotomalala, C., K. Guizien, K. Grangeré, S. Lefebvre, C. Dupuy, and F. Orvain. 2019. Modelling the functioning of a coupled microphytobenthic-EPS-bacterial system in intertidal mudflats. Marine Environmental Research **150**: 104754.

Ralph, P. J., U. Schreiber, R. Gademann, M. Kühl, and A. W. D. Larkum. 2005. Coral photobiology studied with a new imaging pulse amplitude modulated fluorometer. Journal of Phycology **41**: 335–342.

Reible, D., and S. Mohanty. 2002. A levy flight-random walk model for bioturbation.

Environmental Toxicology and Chemistry **21**: 875–881.
Riisgard, H. U. 1991. Suspension feeding in the polychaete Nereis diversicolor. Marine Ecology Progress Series **70**: 29–37.
Rossi, F., A. Baeta, and J. C. Marques. 2015. Stable isotopes reveal habitat-related diet shifts in facultative deposit-feeders. Journal of Sea Research **95**: 172–179.
Saburova, M. A., and I. G. Polikarpov. 2003. Diatom activity within soft sediments: Behavioural and physiological processes. Marine Ecology Progress Series **251**: 115–126.
Saint-Béat, B., C. Dupuy, P. Bocher, J. Chalumeau, M. De Crignis, C. Fontaine, K. Guizien, J. Lavaud, S. Lefebvre, H. Montanié, J. L. Mouget, F. Orvain, P. Y. Pascal, G. Quaintenne, G. Radenac, P. Richard, F. Robin, A. F. Vézina, and N. Niquil. 2013. Key Features of Intertidal Food Webs That Support Migratory Shorebirds. PLoS ONE **8**: 1–17.
Sandwell, D. R., C. A. Pilditch, and A. M. Lohrer. 2009. Density dependent effects of an infaunal suspension-feeding bivalve (Austrovenus stutchburyi) on sandflat nutrient fluxes and microphytobenthic productivity. Journal of Experimental Marine Biology and Ecology **373**: 16–25.
Santos, S., P. C. Luttikhuizen, J. Campos, C. H. R. Heip, and H. W. van der Veer. 2011. Spatial distribution patterns of the peppery furrow shell Scrobicularia plana (da Costa, 1778) along the European coast: A review. Journal of Sea Research **66**: 238–247.
Savelli, R., X. Bertin, F. Orvain, P. Gernez, A. Dale, T. Coulombier, P. Pineau, N. Lachaussée, P. Polsenaere, C. Dupuy, and V. le Fouest. 2019. Impact of Chronic and Massive Resuspension Mechanisms on the Microphytobenthos Dynamics in a Temperate Intertidal Mudflat. Journal of Geophysical Research: Biogeosciences **124**: 3752–3777.
Savelli, R., C. Dupuy, L. Barillé, A. Lerouxel, K. Guizien, A. Philippe, P. Bocher, P. Polsenaere, and V. Le Fouest. 2018. On biotic and abiotic drivers of the microphytobenthos seasonal cycle in a temperate intertidal mudflat: A modelling study. Biogeosciences **15**: 7243–7271.
Scaps, P. 2002. A review of the biology, ecology and potential use of the common ragworm Hediste diversicolor (O.F. Müller) (Annelida: Polychaeta). Hydrobiologia **470**: 203–218.
Serôdio, J. 2003. A chlorophyll fluorescence index to estimate short-term rates of photosynthesis by intertidal microphytobenthos. Journal of Phycology **39**: 33–46.
Serôdio, J. 2004. Analysis of variable chlorophyll fluorescence in microphytobenthos assemblages: Implications of the use of depth-integrated measurements. Aquatic Microbial Ecology **36**: 137–152.
Serôdio, J., J. Ezequiel, A. Barnett, J. L. Mouget, V. Meĺéder, M. Laviale, and J. Lavaud. 2012. Efficiency of photoprotection in microphytobenthos: Role of vertical migration and the xanthophyll cycle against photoinhibition. Aquatic Microbial Ecology **67**: 161–175.
Seuront, L., and N. Spilmont. 2002. Self-organized criticality in intertidal microphytobenthos patch patterns. Physica A: Statistical Mechanics and its Applications **313**: 513–539.
Shnyukova, E. I., and E. K. Zolotareva. 2017. Ecological Role of Exopolysaccharides of Bacillariophyta : A Review. International Journal on Algae **19**: 5–24.
Sommer, U., and F. Sommer. 2006. Cladocerans versus copepods: The cause of contrasting top-down controls on freshwater and marine phytoplankton. Oecologia **147**: 183–194.
Sommer, U., and H. Stibor. 2002. Copepoda - Cladocera - Tunicata: The role of three major mesozooplankton groups in pelagic food webs. Ecological Research **17**: 161–174.
Spilmont, N., L. Seuront, T. Meziane, and D. T. Welsh. 2011. There's more to the picture than meets the eye: Sampling microphytobenthos in a heterogeneous environment. Estuarine, Coastal and Shelf Science **95**: 470–476.
Swanberg, I. L. 1991. The influence of the filter-feeding bivalve Cerastoderma edule L . on

microphytobenthos : a laboratory study. Journal of Experimental Marine Biology and Ecology **151**: 93–111.

Tang, M., and E. Kristensen. 2007. Impact of microphytobenthos and macroinfauna on temporal variation of benthic metabolism in shallow coastal sediments. Journal of Experimental Marine Biology and Ecology **349**: 99–112.

Thrush, S. F., J. E. Hewitt, M. Gibbs, C. Lundquist, and A. Norkko. 2006. Functional role of large organisms in intertidal communities: Community effects and ecosystem function. Ecosystems **9**: 1029–1040.

Tolhurst, T. J., B. Jesus, V. Brotas, and D. M. Paterson. 2003. Diatom migration and sediment armouring - an example from the Tagus Estuary, Portugal. Hydrobiologia **503**: 183–193.

Underwood, G. J. C., and J. C. Kromkamp. 1999. Primary Production by Phytoplankton and Microphytobenthos in Estuaries. Advances in Ecological Research **29**: 93–153.

Vieira, S., L. Ribeiro, B. Jesus, P. Cartaxana, and J. M. Da Silva. 2013a. Photosynthesis assessment in microphytobenthos using conventional and imaging pulse amplitude modulation fluorometry. Photochemistry and Photobiology **89**: 97–102.

Vieira, S., L. Ribeiro, B. Jesus, P. Cartaxana, and J. M. Da Silva. 2013b. Photosynthesis assessment in microphytobenthos using conventional and imaging pulse amplitude modulation fluorometry. Photochemistry and Photobiology **89**: 97–102.

Volkenborn, N., S. A. Woodin, D. S. Wethey, and L. Polerecky. 2016. Bioirrigation in marine sediments, *In* S.A. Elias [ed.], Reference Module in Earth Systems and Environmental Sciences. Elsevier.

Webb, W. L., M. Newton, and D. Starr. 1974. Carbon dioxide exchange of Alnus rubra. Oecologia **17**: 281–291.

Weerman, E. J., P. M. J. Herman, and J. Van De Koppel. 2011. Macrobenthos abundance and distribution on a spatially patterned intertidal flat. Marine Ecology Progress Series **440**: 95–103.

Wolff, W. J. 1973. The estuary as a habitat: an analysis of data on the soft-bottom macrofauna of the estuarine area of the rivers Rhine, Meuse and Scheldt. Zool. Verkan. **126**: 1–242.

Ysebaert, T., and P. M. J. Herman. 2002. Spatial and temporal variation in benthic macrofauna and relationships with environmental variables in an estuarine, intertidal soft-sediment environment. Marine Ecology Progress Series **244**: 105–124.

**Annex: Images of the minimal level of fluorescence (Fo; rel. unit) obtained using imaging-PAM during the experiment (from day 1 to day 6).** The different replicates are represented respectively from R1 to R3. **A1:** the control treatment, **A2 to A4:** treatments with addition of *H. diversicolor* at each density, respectively 249 ind $m^{-2}$, 498 ind $m^{-2}$, and 747 ind $m^{-2}$, and **A5 to A7:** treatments with addition of *S. plana* at each density, respectively 249 ind $m^{-2}$, 338 ind $m^{-2}$, and 498 ind $m^{-2}$.

**A1.** Control treatment

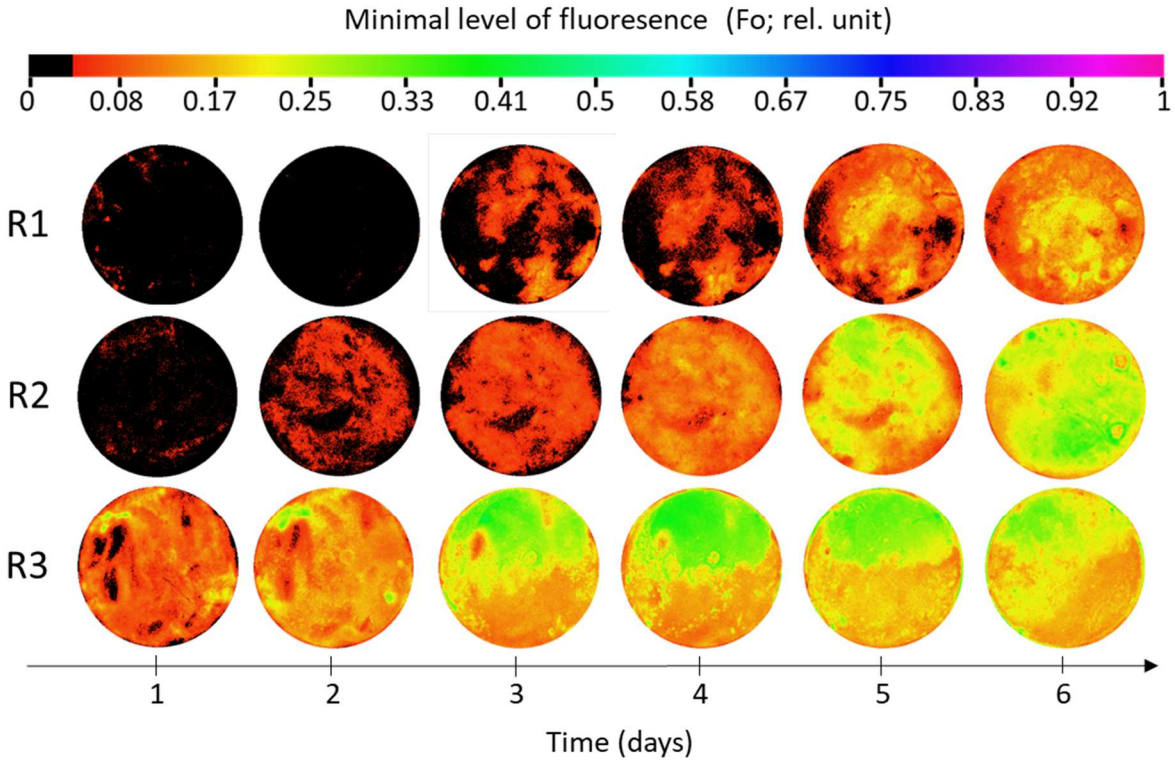


**A2.** Treatment with addition of *Hediste diversicolor* (density = 249 ind $m^{-2}$)

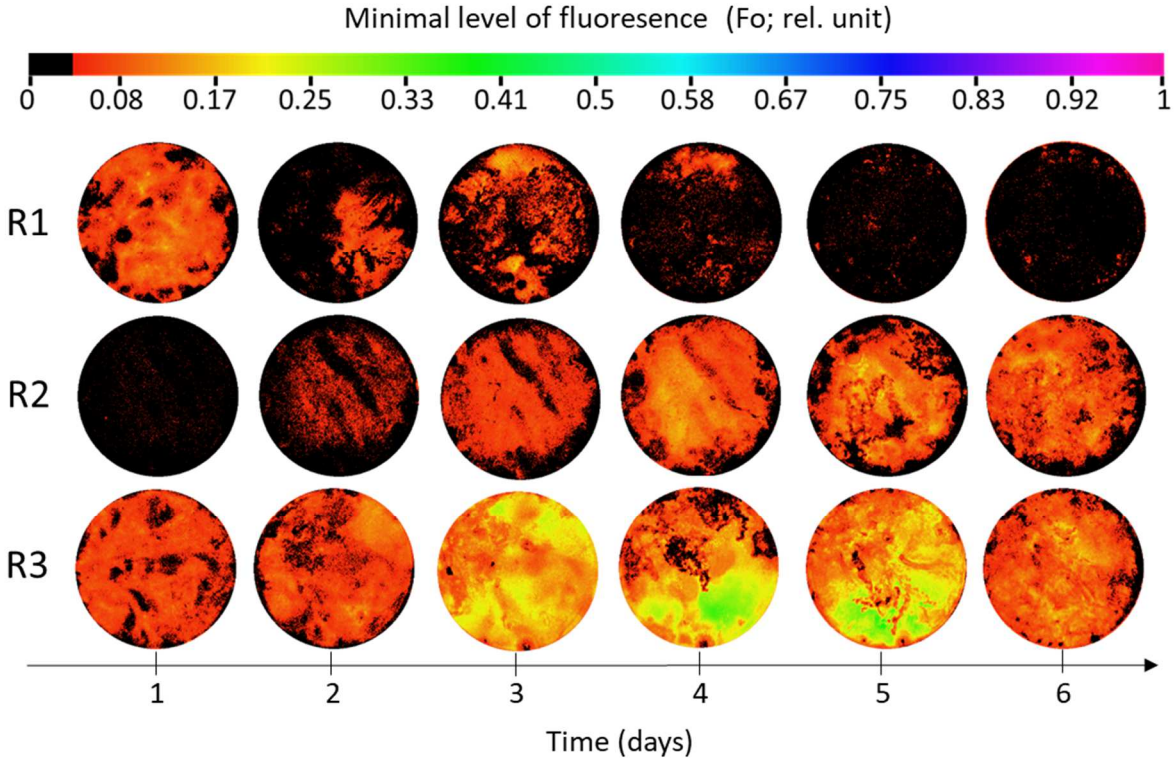

**A3.** Treatment with addition of *Hediste diversicolor* (density = 498 ind $m^{-2}$)

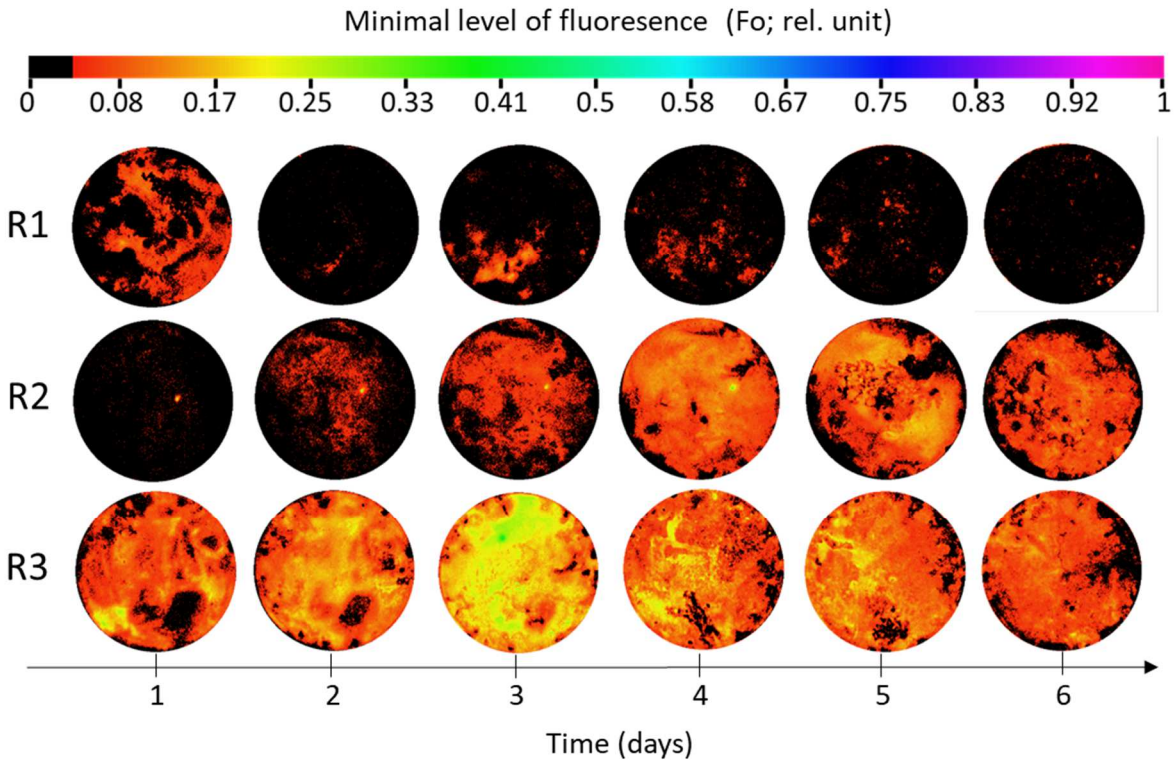


**A4.** Treatment with addition of *Hediste diversicolor* (density = 747 ind $m^{-2}$)

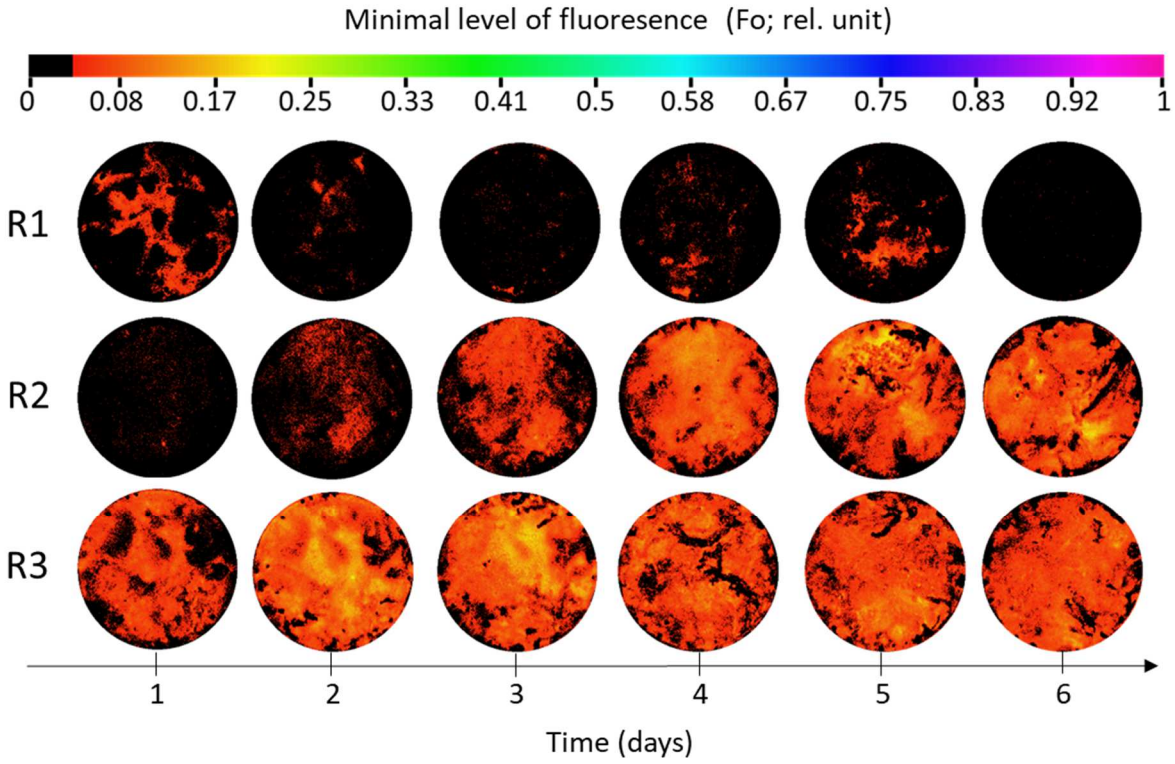

**A5.** Treatment with addition of *Scrobicularia plana* (density = 249 ind $m^{-2}$)

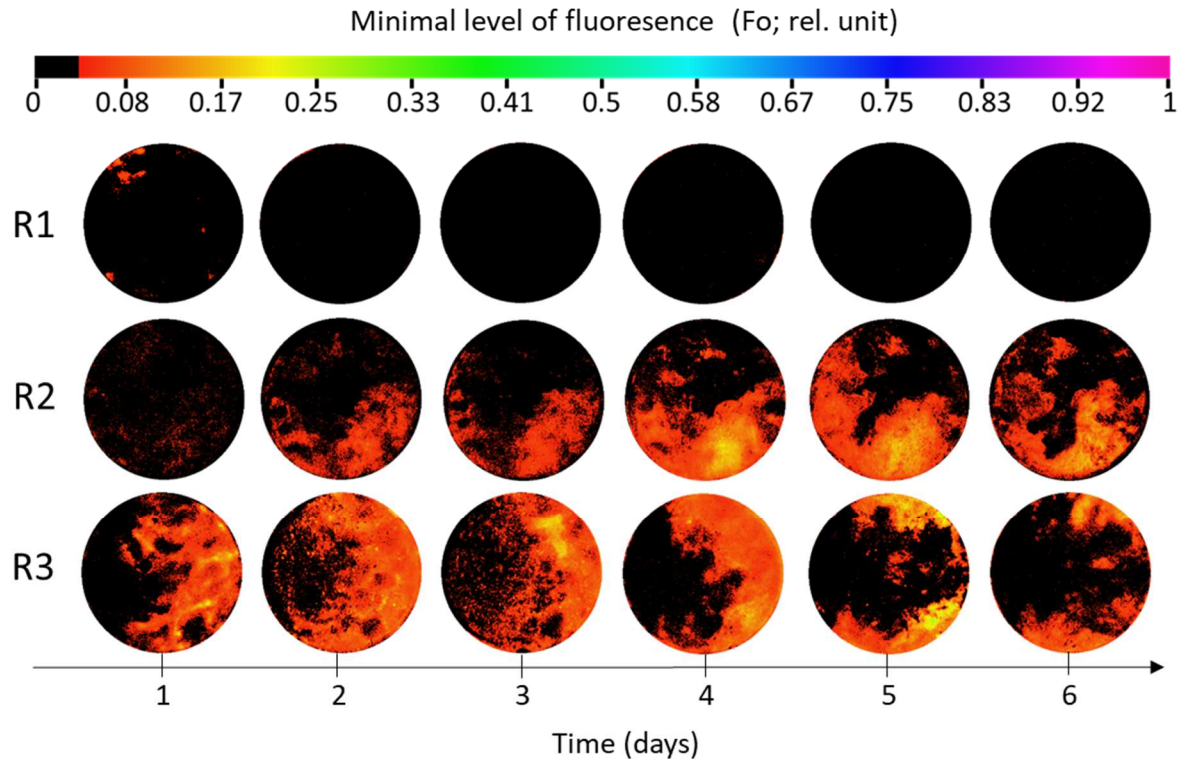


**A6.** Treatment with addition of *Scrobicularia plana* (density = 338 ind $m^{-2}$)

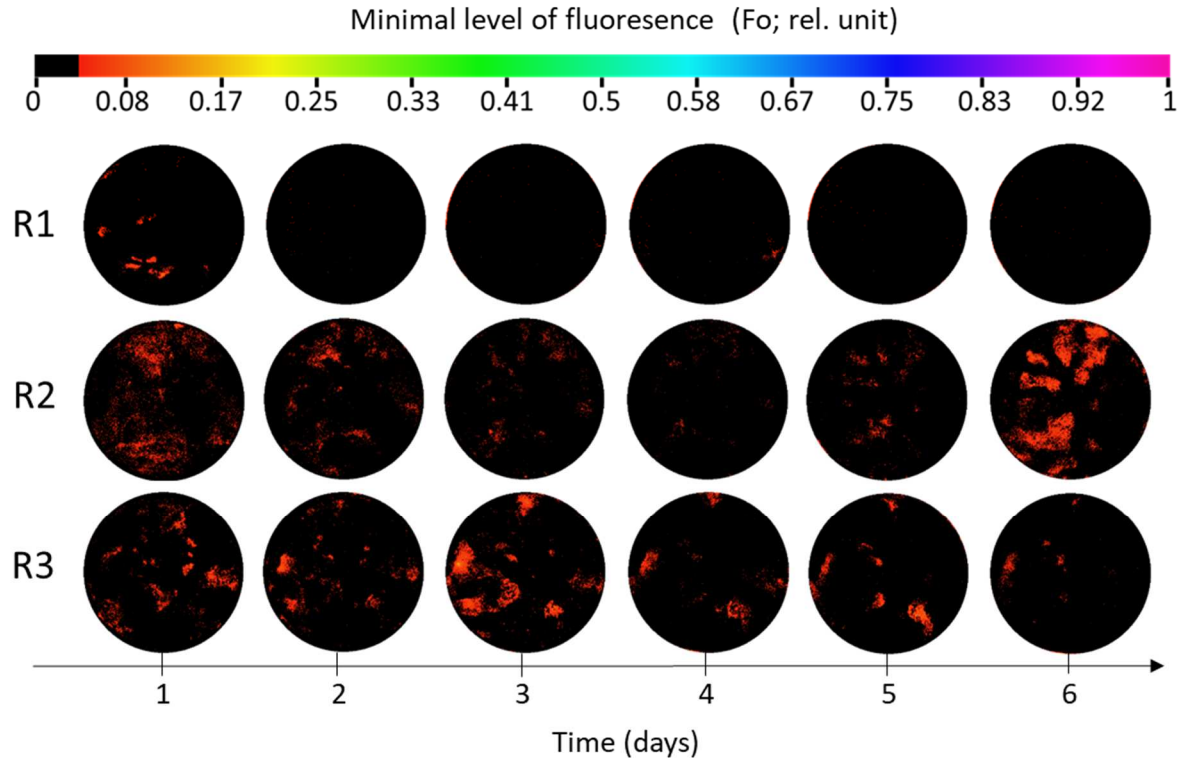

**A7.** Treatment with addition of *Scrobicularia plana* (density = 498 ind $m^{-2}$)